nature reviews physics

https://doi.org/10.1038/s42254-024-00795-0

Technical review

Check for updates

Phonon-limited electronic transport through first principles

Romain Claes [1,2], Samuel Poncé [1,3], Gian-Marco Rignanese [1,3,4] & Geoffroy Hautier [5]

Abstract

Understanding electronic transport in materials is essential to both fundamental and applied physics, as it directly influences critical properties such as the mobility of semiconductors and the efficiency of thermoelectric materials. Electron transport hinges on electronic structure of a material and various scattering events. Among these, scattering by phonons stands out as one of the most fundamental mechanisms, as it occurs even in pristine single crystals. But only recently have advances in the development of accurate first-principles methods allowed the precise calculation of electronic transport properties entirely from first principles, without relying on experimental parameters. This Technical Review presents the underlying physics of phonon-limited linear transport, primarily within the framework of the Boltzmann transport formalism but also for alternative approaches, such as the Landauer–Büttiker and Kubo frameworks. In addition, this Review covers technical aspects of implementing these formalisms, including their limitations and the scope of their applicability. Finally, we will discuss some specific transport regimes, such as transport in a strong electric field or involving the effect of spin–orbit coupling.

Sections

[1]European Theoretical Spectroscopy Facility, Institute of Condensed Matter and Nanosciences, UCLouvain, Louvain-la-Neuve, Belgium. [2]School of Chemistry, University of Birmingham, Edgbaston, Birmingham, UK. [3]WEL Research Institute, Wavre, Belgium. [4]School of Materials Science and Engineering, Northwestern Polytechnical University, Shaanxi, P. R. China. [5]Thayer School of Engineering, Dartmouth College, Hanover NH, USA. e-mail: geoffroy.hautier@dartmouth.edu

Key points

- Accurate phonon-limited transport methodologies are crucial for predicting material performance, as electron–phonon interactions impact key properties such as mobility, Hall factor and thermoelectric efficiency.
- The main approaches for phonon-limited transport modelling are the Boltzmann transport equation, Kubo formalism and Landauer–Büttiker approach, each suited to specific transport conditions and system scales.
- These first-principles methods enable accurate calculations of electronic transport properties without relying on empirical parameters, allowing the prediction of new materials.
- Transport behaviour can become particularly complex in certain regimes involving, for example, non-equilibrium phonons, high electric fields, low dimensionality or spin–orbit coupling effects, each introducing their own specificities.

Introduction

The understanding and computation of carrier transport in materials play a pivotal role in both fundamental and applied physics, as they control important properties such as thermoelectric efficiency and semiconductor mobility. The mobility quantifies how fast charge carriers — holes or electrons — can travel in a material under the influence of an external electric field **E**. When an electric field is applied to a doped semiconductor or a metal, electrons and holes begin to flow along this field. The change in carrier occupation resulting from the electric field defines the carrier mobility. Using the semiclassical Drude model, carrier mobility takes the simple form $\mu = e\tau/m^*$. In this expression, the effective mass of the carriers m^* is directly linked to their velocity in the solid and their lifetime τ describes the average time between two scattering events. Multiple scattering mechanisms can coexist in materials, such as those from intrinsic interplay with phonons and other mobile charges, and to extrinsic interactions with impurities, defects and grain boundaries. Among these, both intrinsic mechanisms occur even in pure single crystals, and electron–phonon scattering is particularly significant at room and higher temperature. This Review focuses primarily on electron–phonon scattering.

Over the past decade, substantial progress has been achieved in the development of sophisticated first-principles approaches and codes. These advances have enabled the calculation of carrier transport properties, including conductivity, mobility and the Seebeck coefficient, directly from first principles. The fundamental physics underlying phonon-limited transport can be described using various methodologies. The different types of transport phenomena and codes mentioned in this Review are presented in Fig. 1. Here, we will primarily review the intrinsic transport regime from weak electron–phonon coupling.

Our main focus will revolve around the widely used Boltzmann transport formalism, which elucidates the behaviour of charge carriers within a solid as they respond to an applied electric field. In this framework, carriers are characterized as wave packets that follow equations of motion between successive scattering events. Next, we will review alternative methodologies, including the Kubo formalism, which interprets transport in terms of the linear response of material to time-dependent external perturbations and the Landauer(–Büttiker) method, which addresses transport as a ballistic problem. We will start with the most common transport regimes and move to more specific regimes, considering the impact of out-of-equilibrium phonons, low dimensionality, high electric field, surrounding dielectrics or spin–orbit effects. We will present the theoretical framework of all methods, report on the different codes available and discuss their strengths and weaknesses.

Electron–phonon scattering in the standard regime

Physics of the scattering of electrons by phonons

Describing phonon-limited transport remains a complex task, especially determining the scattering rates involved. One of the first attempts to address this challenge was a discussion of the interaction between electrons and the 'elastic waves of the lattice' — the concept of 'phonons' had not yet been defined in 1929 (ref. 1). Since then, several phenomenological approaches have been developed to further understand the interactions between electrons and phonons. These approaches aim to break down the overall electron–phonon interaction into different contributions, such as acoustic and optical deformation potential scattering or polar optical phonon scattering. In the past two decades, the emergence of accurate theoretical methods and codes that allow for the computation of electronic transport quantities from first principles, without relying on any experimental parameters, has driven much progress. These advances have also enabled researchers to move beyond the simplistic view offered by the Drude model and to overcome the limitations associated with working exclusively with systems characterized by a single parabolic band. All these advancements have opened up opportunities to explore and gain a deeper understanding of electronic transport phenomena in materials.

We will start our Review by discussing the most common conditions that we will call the standard regime. As outlined in Fig. 1, it assumes phonons being in equilibrium, weak electron–phonon coupling, low electric field and no magnetism or spin effect. These are the most common assumptions in the field, for which methods and codes are widely available. Within these constraints, there are three main theoretical schemes: the Boltzmann transport equation (BTE), the Kubo and the Landauer–Büttiker frameworks.

Boltzmann transport equation

By far the most widely used method relies on the BTE, which describes the carrier transport and the different scattering events that limit it in a diffusive regime. Following Fig. 1, we first describe the BTE in the standard drift regime, before briefly exploring a more specific regime in which the application of a magnetic field gives rise to Hall transport — a property widely studied experimentally. Within the BTE method, several approximations are available, which we will describe and discuss. We will also present the different interpolation approaches used to obtain the electron–phonon quantities before moving to empirical models that allow the fast computation of transport properties within the BTE formalism.

In this Review, we focus on the final equations of the BTE. Their derivation can be found in refs. 2–5. We consider the case of electrons only, but similar expressions exist for holes. A central observable in the BTE method is the current density, which expresses the number of electrons crossing a unit area per unit of time and can be written as

$$J_\alpha = \frac{-1}{\Omega} \sum_{n \in CB} \int \frac{d\mathbf{k}}{\Omega_{BZ}} f_{n\mathbf{k}}(\mathbf{E}) v_{n\mathbf{k},\alpha}. \quad (1)$$

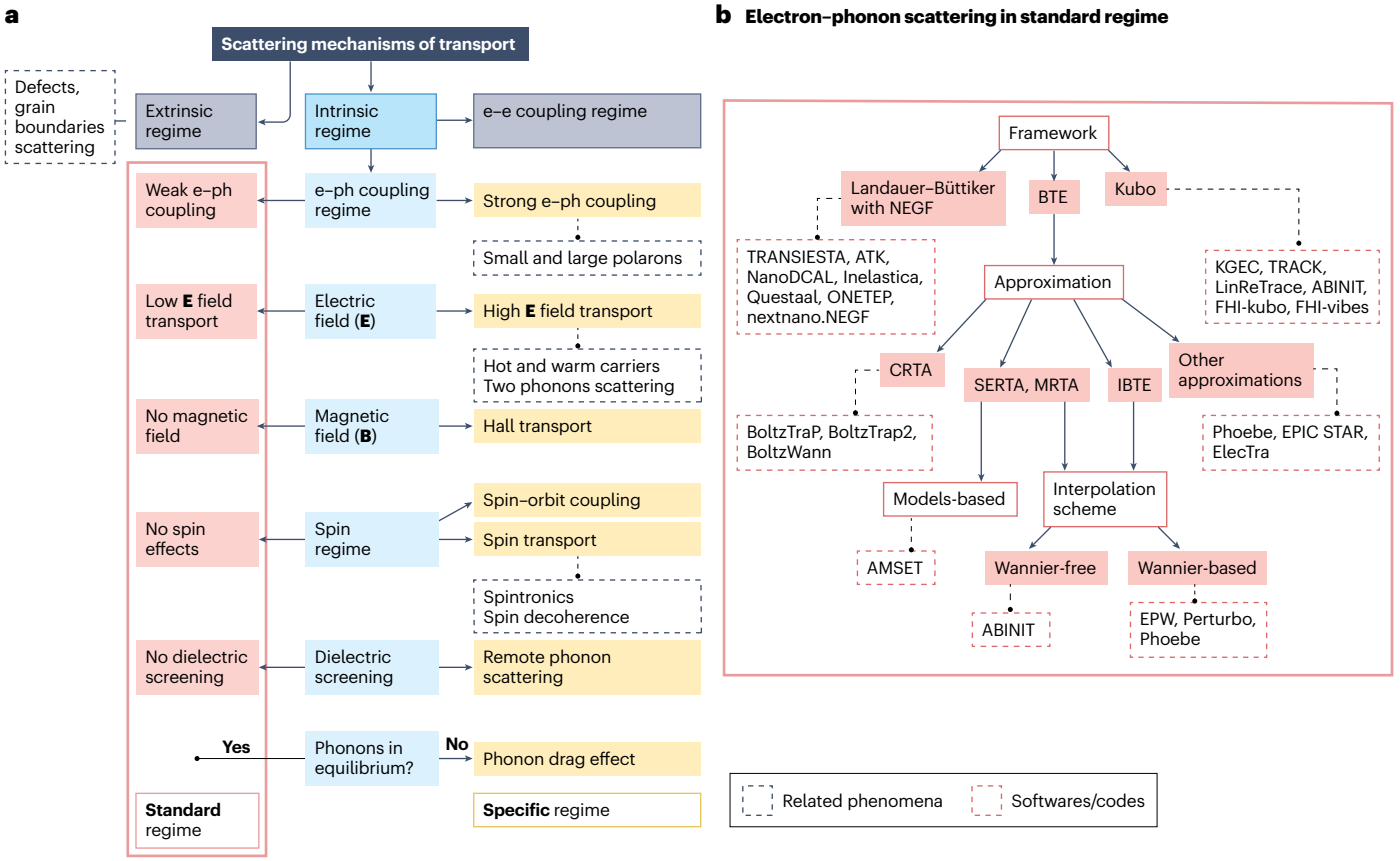

Fig. 1 | Roadmap of this Review. a, Carrier transport broadly falls into two regimes: the extrinsic regime and the intrinsic regime. This Review focuses on the intrinsic regime owing to electron–phonon scattering, starting with the standard regime (red) before moving to more specific regimes linked to different phenomena. **b**, To model electron–phonon scattering in the standard regime, different frameworks, approximations and codes can be used. NEGF means the non-equilibrium Green's function approach, BTE the Boltzmann transport equation, CRTA the constant relaxation-time approximation, SERTA the self-energy relaxation-time approximation, MRTA the momentum relaxation-time approximation and IBTE the iterative Boltzmann transport equation, and e–ph stands for electron–phonon and e–e for electron–electron. The different softwares mentioned are `TRANSIESTA`[108], `NanoDCAL`[114,115], `Inelastica`[109–112], `Questaal`[116], `ONETEP`[118,119], `ATK`[113], `nextnano.NEGF`[117], `KGEC`[88], `FHI-kubo`[84], `FHI-vibes`[90], `TRACK`[81], `LinReTraCe`[74], `ABINIT`[46,47,87], `BoltzTraP`[23], `BoltzTraP2`[24], `BoltzWann`[25], `AMSET`[12], `EPW`[20], `PERTURBO`[38], `PHOEBE`[15], `EPIC STAR`[37] and `ElecTra`[237].

In this equation, $f_{n\mathbf{k}}(\mathbf{E})$ is the occupation function of a given state $n\mathbf{k}$, in which n is the band index in the conduction band (CB) and $\mathbf{k}$ the wave vector, Ω and Ω_{BZ} refer, respectively, to the volume of the unit cell and first Brillouin zone, and α stands for the Cartesian coordinates. As electrons are moving in the opposite direction to the current density, the latter takes on a negative sign. Finally, $v_{n\mathbf{k},\alpha}$ is the velocity of the electrons defined as $\mathbf{v}_{n\mathbf{k}} = \nabla_{\mathbf{k}}\varepsilon_{n\mathbf{k}}$, with $\varepsilon_{n\mathbf{k}}$ describing the corresponding band structure of the material[2,3,6,7].

As the electron mobility is defined as the derivative of the current with respect to the electric field $\mathbf{E}$, we obtain

$$\mu_{e,\alpha\beta} = \frac{-1}{\Omega n_e} \sum_{n\in CB} \int \frac{d\mathbf{k}}{\Omega_{BZ}} \frac{\partial f_{n\mathbf{k}}(\mathbf{E})}{\partial \mathbf{E}_\beta}\bigg|_{\mathbf{E}=0} v_{n\mathbf{k},\alpha}, \quad (2)$$

in which n_e is the electron concentration. Knowledge of $f_{n\mathbf{k}}(\mathbf{E})$ is crucial to evaluate the mobility, as it is for the current density.

Assuming a system with no change in temperature and a time-independent electric field, the evolution of $f_{n\mathbf{k}}(\mathbf{E})$ with time can be described by three terms: the in-diffusion and out-diffusion of the carriers (D), the external forces (F) and the scattering of the carriers (S). As $f_{n\mathbf{k}}(\mathbf{E})$ does not vary with time in the steady state, we obtain the BTE by adding up the different contributions[4,5]:

$$\frac{\partial f_{n\mathbf{k}}(\mathbf{E})}{\partial t} = 0 = \left(\frac{\partial f_{n\mathbf{k}}(\mathbf{E})}{\partial t}\right)_D + \left(\frac{\partial f_{n\mathbf{k}}(\mathbf{E})}{\partial t}\right)_F + \left(\frac{\partial f_{n\mathbf{k}}(\mathbf{E})}{\partial t}\right)_S. \quad (3)$$

In this equation, the change of $f_{n\mathbf{k}}(\mathbf{E})$ owing to carrier diffusion is null as we assume the distribution function to be homogeneous. In the case of external forces (F), we can consider two distinct scenarios: the influence of an electric field only, resulting in the so-called drift mobility; and the combined impact of both an electric and a magnetic field ($f_{n\mathbf{k}}(\mathbf{E},\mathbf{B})$), giving rise to Hall mobility.

Drift transport. The change of $f_{n\mathbf{k}}(\mathbf{E})$ owing to an electric field only can be expressed as[2,4,5]:

$$\left(\frac{\partial f_{n\mathbf{k}}(\mathbf{E})}{\partial t}\right)_F = -\frac{\partial \mathbf{k}}{\partial t} \cdot \nabla_{\mathbf{k}} f_{n\mathbf{k}}(\mathbf{E}) = \mathbf{E} \cdot \nabla_{\mathbf{k}} f_{n\mathbf{k}}(\mathbf{E}). \quad (4)$$

Therefore, equation (3) now becomes

$$-\left(\frac{\partial f_{n\mathbf{k}}(\mathbf{E})}{\partial t}\right)_{\mathrm{F}} = -\mathbf{E}\cdot\nabla_{\mathbf{k}} f_{n\mathbf{k}}(\mathbf{E}) = \left(\frac{\partial f_{n\mathbf{k}}(\mathbf{E})}{\partial t}\right)_{\mathrm{S}}. \tag{5}$$

Without any electrical field, the occupation function $f_{n\mathbf{k}}(\mathbf{E})$ reduces to the Fermi–Dirac distribution, which is defined by $f^0_{n\mathbf{k}} = 1/(e^{(\varepsilon_{n\mathbf{k}}-\varepsilon_{\mathrm{F}})/k_{\mathrm{B}}T}+1)$, in which T is the temperature, k_{B} is the Boltzmann constant, ε_{F} is the Fermi level and $\varepsilon_{n\mathbf{k}}$ is the energy of an electron in the state $n\mathbf{k}$. Here, we consider a small electrical field, which implies that $f_{n\mathbf{k}}(\mathbf{E})$ is relatively close to the equilibrium Fermi–Dirac distribution. Using the low-field regime, we can therefore approximate $\mathbf{E}\nabla_{\mathbf{k}} f_{n\mathbf{k}}(\mathbf{E}) \approx \mathbf{E}\nabla_{\mathbf{k}} f^0_{n\mathbf{k}}(\mathbf{E})$. Using the definition of the velocity, we find

$$\nabla_{\mathbf{k}} f^0_{n\mathbf{k}} = \frac{\partial f^0_{n\mathbf{k}}}{\partial\varepsilon}\nabla_{\mathbf{k}}\varepsilon_{n\mathbf{k}} = \frac{\partial f^0_{n\mathbf{k}}}{\partial\varepsilon}\mathbf{v}_{n\mathbf{k}} \tag{6}$$

and finally, we obtain the linearized BTE:

$$-\mathbf{E}\cdot\mathbf{v}_{n\mathbf{k}}\frac{\partial f^0_{n\mathbf{k}}}{\partial\varepsilon} = \left(\frac{\partial f_{n\mathbf{k}}}{\partial t}\right)_{\mathrm{S}}. \tag{7}$$

In a solid, several mechanisms can cause the scattering of electrons: extrinsic mechanisms such as defects or grain boundaries and intrinsic mechanisms owing to electron–phonon or electron–electron interactions. In this Review, we focus on the intrinsic scattering by phonons, which does not rely on the quality of the sample studied. It is the most important mechanism at room temperature (and higher), where the vibrations of the atoms are already significant. Consequently, four processes can take place, as determined by Fermi's golden rule: out-of-state transitions in which electrons in state $n\mathbf{k}$ can go to state $m\mathbf{k}+\mathbf{q}$ – either by absorbing or by emitting a phonon $\omega_{\mathbf{q}\nu}$ – or in-state transitions in which electrons in state $m\mathbf{k}+\mathbf{q}$ can either emit or absorb a phonon $\omega_{\mathbf{q}\nu}$ to go to state $n\mathbf{k}$ (refs. 2,3). It is therefore crucial to have a phonon of a specific energy and momentum to allow a precise energy transition.

Figure 2 illustrates the need for three completely distinct phonon modes to enable different electronic transitions in silicon. The intra-valley transitions in blue and yellow require phonons of small momentum but of different energies, whereas the inter-valley transition is associated with a phonon that allows a larger momentum change. The probability that a given phonon allows the transition between two states is determined by the square of the electron–phonon coupling matrix elements, $g_{mn\nu}(\mathbf{k},\mathbf{q})$. Therefore, equation (7) becomes[2]

$$\begin{aligned}-\mathbf{E}\cdot\mathbf{v}_{n\mathbf{k}}\frac{\partial f^0_{n\mathbf{k}}}{\partial\varepsilon} = 2\pi\sum_{m,\nu}\int_{\mathrm{BZ}}\frac{d\mathbf{q}}{\Omega_{\mathrm{BZ}}}|g_{mn\nu}(\mathbf{k},\mathbf{q})|^2 \\ \times[(1-f_{n\mathbf{k}})f_{m\mathbf{k}+\mathbf{q}}\delta(\varepsilon_{n\mathbf{k}}-\varepsilon_{m\mathbf{k}+\mathbf{q}}+\omega_{\mathbf{q}\nu})(1+n_{\mathbf{q}\nu}) \\ +(1-f_{n\mathbf{k}})f_{m\mathbf{k}+\mathbf{q}}\delta(\varepsilon_{n\mathbf{k}}-\varepsilon_{m\mathbf{k}+\mathbf{q}}-\omega_{\mathbf{q}\nu})n_{\mathbf{q}\nu} \\ -f_{n\mathbf{k}}(1-f_{m\mathbf{k}+\mathbf{q}})\delta(\varepsilon_{n\mathbf{k}}-\varepsilon_{m\mathbf{k}+\mathbf{q}}-\omega_{\mathbf{q}\nu})(1+n_{\mathbf{q}\nu}) \\ -f_{n\mathbf{k}}(1-f_{m\mathbf{k}+\mathbf{q}})\delta(\varepsilon_{n\mathbf{k}}-\varepsilon_{m\mathbf{k}+\mathbf{q}}+\omega_{\mathbf{q}\nu})n_{\mathbf{q}\nu}],\end{aligned} \tag{8}$$

in which δ is the Dirac delta function and $n_{\mathbf{q}\nu}$ is the Bose–Einstein distribution. The Dirac delta function effectively sets a constraint on energy and momentum conservation. In numerical implementations, it is convenient to replace this δ distribution by a Lorentzian or a Gaussian using a small broadening parameter, an adaptive broadening[8] or using a linear tetrahedron method as proposed by Blöchl et al.[9], which bypasses the need for a convergence study on the broadening parameter. We note that these numerical integration methods can fail in piezoelectric materials, requiring a specific self-consistent treatment to reach convergence[10].

The electron–phonon matrix elements $g_{mn\nu}(\mathbf{k},\mathbf{q})$ can be expressed as

$$g_{mn\nu}(\mathbf{k},\mathbf{q}) = \left\langle u^{\mathrm{KS}}_{m\mathbf{k}+\mathbf{q}}\middle|\Delta_{\mathbf{q}\nu}V^{\mathrm{KS}}\middle|u^{\mathrm{KS}}_{n\mathbf{k}}\right\rangle, \tag{9}$$

in which $u^{\mathrm{KS}}_{n\mathbf{k}}$ and $u^{\mathrm{KS}}_{m\mathbf{k}+\mathbf{q}}$ are the Bloch-periodic components of the Kohn–Sham electron wavefunctions and $\Delta_{\mathbf{q}\nu}V^{\mathrm{KS}}$ is the phonon-induced variation of the self-consistent potential experienced by electrons[6,7,11]. In other words, if the initial state wavefunction $u^{\mathrm{KS}}_{n\mathbf{k}}$ perturbed by the phonon is similar to the final state wavefunction $u^{\mathrm{KS}}_{m\mathbf{k}+\mathbf{q}}$, the transition has a high probability and therefore $g_{mn\nu}(\mathbf{k},\mathbf{q})$ is important.

By taking the derivatives of each side of equation (8) with respect to the electric field $\mathbf{E}$, we obtain

$$\begin{aligned}\left.\frac{\partial f_{n\mathbf{k}}(\mathbf{E})}{\partial\mathbf{E}_\beta}\right|_{\mathbf{E}=0} = \frac{\partial f^0_{n\mathbf{k}}}{\partial\varepsilon_{n\mathbf{k}}}v_{n\mathbf{k},\beta}\tau^0_{n\mathbf{k}} + 2\pi\tau^0_{n\mathbf{k}}\sum_{m,\nu}\int\frac{d\mathbf{q}}{\Omega_{\mathrm{BZ}}}|g_{mn\nu}(\mathbf{k},\mathbf{q})|^2 \\ \times[(1+n_{\mathbf{q}\nu}-f^0_{n\mathbf{k}})\delta(\varepsilon_{n\mathbf{k}}-\varepsilon_{m\mathbf{k}+\mathbf{q}}+\omega_{\mathbf{q}\nu}) \\ +(n_{\mathbf{q}\nu}+f^0_{n\mathbf{k}})\delta(\varepsilon_{n\mathbf{k}}-\varepsilon_{m\mathbf{k}+\mathbf{q}}-\omega_{\mathbf{q}\nu})]\left.\frac{\partial f_{m\mathbf{k}+\mathbf{q}}(\mathbf{E})}{\partial E_\beta}\right|_{\mathbf{E}=0},\end{aligned} \tag{10}$$

with the relaxation time $\tau^0_{n\mathbf{k}}$ defined as

$$\begin{aligned}\frac{1}{\tau^0_{n\mathbf{k}}} = 2\pi\sum_{m,\nu}\int\frac{d\mathbf{q}}{\Omega_{\mathrm{BZ}}}|g_{mn\nu}(\mathbf{k},\mathbf{q})|^2 \\ \times[(n_{\mathbf{q}\nu}+f^0_{m\mathbf{k}+\mathbf{q}})\delta(\varepsilon_{n\mathbf{k}}-\varepsilon_{m\mathbf{k}+\mathbf{q}}+\omega_{\mathbf{q}\nu}) \\ +(n_{\mathbf{q}\nu}+1-f^0_{m\mathbf{k}+\mathbf{q}})\delta(\varepsilon_{n\mathbf{k}}-\varepsilon_{m\mathbf{k}+\mathbf{q}}-\omega_{\mathbf{q}\nu})],\end{aligned} \tag{11}$$

and equation (2) can therefore be used to obtain the mobility. However, the main problem in solving equation (10) lies in the interdependence between $\frac{\partial f_{n\mathbf{k}}(\mathbf{E})}{\partial\mathbf{E}_\beta}$ (initial state $n\mathbf{k}$) and $\frac{\partial f_{m\mathbf{k}+\mathbf{q}}(\mathbf{E})}{\partial\mathbf{E}_\beta}$ (final state $m\mathbf{k}+\mathbf{q}$). This system of linear equations needs to be solved iteratively but for years solving the iterative Boltzmann transport equation (IBTE) has been disregarded in favour of methods based on approximations because there was no numerical implementation of the full IBTE[2,3,6,12,13], as shown in Fig. 1. We will discuss these approximations subsequently. Apart from the IBTE solver, several alternative approaches exist to solve the BTE exactly, such as the variational[14,15] and relaxons solvers[15] or the Rode iterative method[16,17].

Hall transport. From an experimental perspective, drift mobility is rarely measured directly. Instead, Hall measurements are typically preferred owing to their simplicity and often higher accuracy. These Hall measurements are conducted under the additional influence of an external magnetic field $\mathbf{B}$, which exerts a supplementary Lorentz force on the charge carriers, altering their mobility. As a result, the BTE needs to be extended to include a new term that characterizes the behaviour of charge carriers in the presence of a magnetic field to be compared with these measurements. Therefore, equation (10) becomes[2,18,19]

$$\begin{aligned}[1-\tau_{n\mathbf{k}}(v_{n\mathbf{k}}\times\mathbf{B})\cdot\nabla_{\mathbf{k}}]\left.\frac{\partial f_{n\mathbf{k}}}{\partial E_\beta}(\mathbf{E},\mathbf{B})\right|_{\mathbf{E}=0} \\ = \frac{\partial f^0_{n\mathbf{k}}}{\partial\varepsilon_{n\mathbf{k}}}v_{n\mathbf{k},\beta}\tau^0_{n\mathbf{k}} + 2\pi\tau^0_{n\mathbf{k}}\sum_{m,\nu}\int\frac{d\mathbf{q}}{\Omega_{\mathrm{BZ}}}|g_{mn\nu}(\mathbf{k},\mathbf{q})|^2 \\ \times[(1+n_{\mathbf{q}\nu}-f^0_{n\mathbf{k}})\delta(\varepsilon_{n\mathbf{k}}-\varepsilon_{m\mathbf{k}+\mathbf{q}}+\omega_{\mathbf{q}\nu}) \\ +(n_{\mathbf{q}\nu}+f^0_{n\mathbf{k}})\delta(\varepsilon_{n\mathbf{k}}-\varepsilon_{m\mathbf{k}+\mathbf{q}}-\omega_{\mathbf{q}\nu})]\left.\frac{\partial f_{m\mathbf{k}+\mathbf{q}}}{\partial E_\beta}(\mathbf{E},\mathbf{B})\right|_{\mathbf{E}=0}.\end{aligned} \tag{12}$$

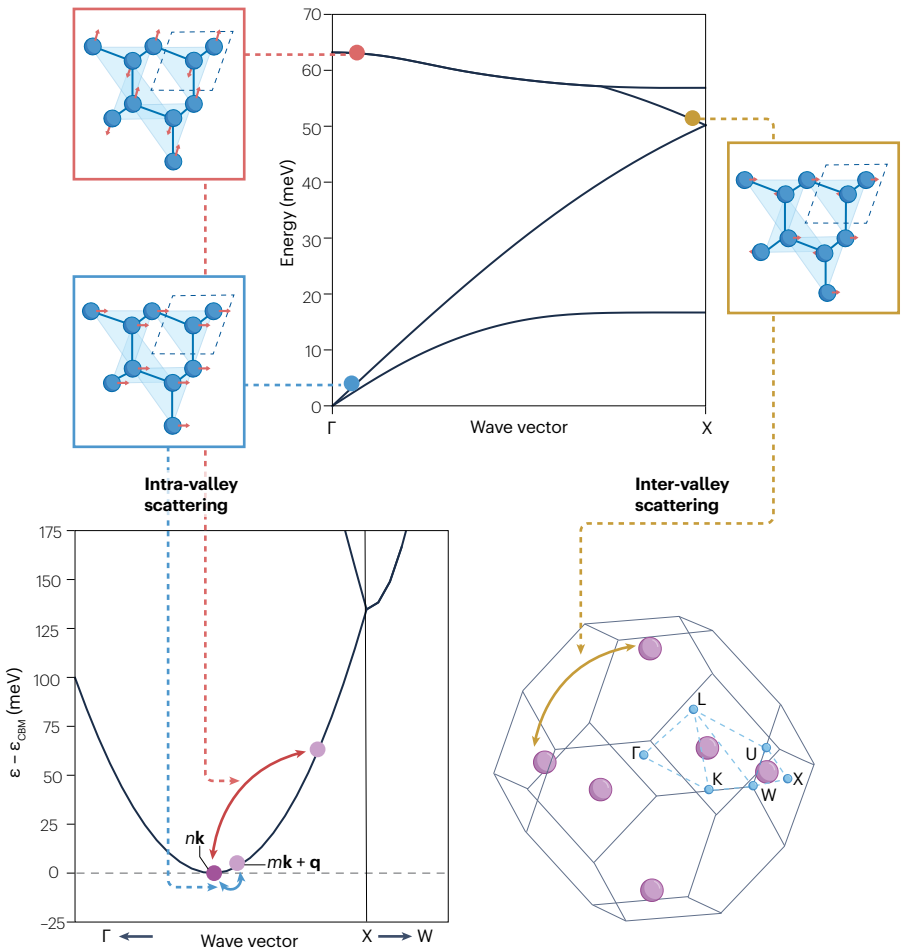

Fig. 2 | Schematic representation of intra-valley and inter-valley transitions in silicon. The intra-valley transitions (red, blue) of an electron occur from a state $n\mathbf{k}$ to two different states $m\mathbf{k}+\mathbf{q}$ by absorption or emission of two different phonons $\mathbf{q}\nu$ of small momentum, and the inter-valley transition (yellow) happens between two different electron pockets owing to a phonon of larger $\mathbf{q}$. The top panel depicts the phonon dispersion of Si between the Γ and X points. The bottom left panel illustrates a zoom-in of the electronic band structure on the conduction band minimum, and the bottom right panel shows the Fermi surface at an energy level close to the conduction band minimum showing the different electronic pockets (purple).

As we consider small magnetic fields, their effect on the electronic and vibrational properties can be disregarded and evaluated at $\mathbf{B}=0$. When a magnetic field is applied in the direction $\hat{\mathbf{B}}$, it induces an orthogonal flow of charge carriers that can be described using the linear response of the mobility to this magnetic field[19,20]

$$\mu^{(2)}_{\alpha\beta}(\hat{\mathbf{B}}) = -\lim_{\mathbf{B}\to 0}\frac{1}{|\mathbf{B}|}\left[\frac{1}{n_e\Omega}\sum_n\int\frac{d\mathbf{k}}{\Omega_{\mathrm{BZ}}}v_{n\mathbf{k},\alpha}\frac{\partial f_{nk}}{\partial E_\beta}(\mathbf{B})-\mu_{\alpha\beta}\right]. \quad (13)$$

Therefore, we can link the Hall mobility μ^{H} directly to the drift mobility μ using the Hall factor r^{H} following

$$\mu^{\mathrm{H}}_{\alpha\beta}(\hat{\mathbf{B}}) = \sum_\gamma r^{\mathrm{H}}_{\alpha\gamma}(\hat{\mathbf{B}})\mu_{\gamma\beta}, \quad (14)$$

with the dimensionless Hall factor defined as[19,20]

$$r^{\mathrm{H}}_{\alpha\gamma}(\hat{\mathbf{B}}) = \sum_{\gamma\delta}\mu^{-1}_{\alpha\gamma}\mu^{(2)}_{\gamma\delta}(\hat{\mathbf{B}})\mu^{-1}_{\delta\beta}. \quad (15)$$

The Hall factor is material-dependent and also varies with the intensity of the magnetic field, the temperature and the doping of the material. Usually, r^{H} varies between 0.7 and 1.9 at room temperature but can change considerably with temperature[19]. For example, a value around 1.15 is found for bulk Si and GaAs at 500K (refs. 19,21). This Hall factor can be obtained experimentally from the Hall coefficient R^{H} measured in a Hall effect experiment[22]

$$R^{\mathrm{H}} = \frac{E_y}{(j_x B)} = \frac{\mu^{\mathrm{H}}}{\sigma} = \frac{1}{en}r^{\mathrm{H}}. \quad (16)$$

This Hall coefficient is often used experimentally to determine the number and the nature of the carriers that conduct the current inside a material: a negative (positive) R^{H} indicates electron (hole) conduction[22].

Approximations to the BTE. One of the easiest ways to bypass the iterative part of equation (10) (or equation (12) in the case of Hall transport) is by making the simplifying assumption that all relaxation times $\tau_{n\mathbf{k}}$ are equal to the same constant for all states ($\tau_{n\mathbf{k}}=\tau$). This approach, known as the constant relaxation-time approximation (CRTA), fixes the relaxation time τ, rendering the mobility dependent solely on the band structure. Consequently, there is no need to calculate the expensive electron–phonon matrix elements, drastically reducing the required computational resources. The CRTA has found widespread applications in various contexts and is, for example, implemented in the `BoltzTraP`[23,24] and `BoltzWann` software[25]. In fact, it has been extensively employed to effectively mimic and comprehend experimental results by fitting the relaxation time to match the experimental data[24,26,27]. The CRTA has also been used in high-throughput

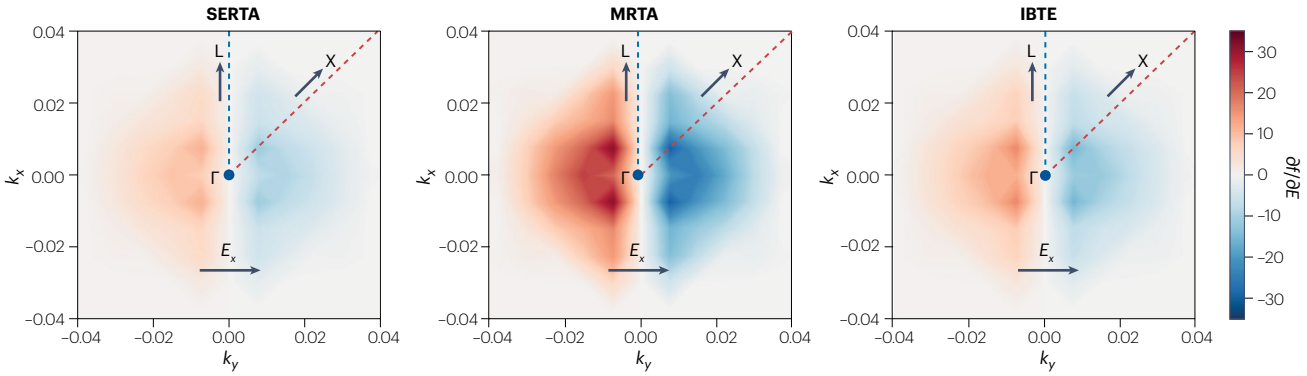

Fig. 3 | Comparison of different approaches to solve the Boltzmann transport equation. Variation of the linear response coefficients, $\partial f/\partial E$, in the (001) plane of the Brillouin zone of MgO owing to an electric field E_x (in the x direction) for the two approximations — self-energy relaxation-time approximation (SERTA) and momentum relaxation-time approximation (MRTA) — and solving the iterative Boltzmann transport equation (IBTE).

studies, enabling the ranking of large sets of materials using a common lifetime[28–31] or, equivalently, by evaluating the transport effective mass[32,33].

Although the ranking based on effective mass or Seebeck coefficient demonstrates a strong correlation with experimental results[29,34], as these two parameters are not directly influenced by the carrier lifetime in the CRTA, the ranking based on conductivity or mobility exhibits a considerably weaker alignment with both experimental data[34] and the exact IBTE solution[13]. Thus, although the CRTA offers computational advantages, it is essential to exercise caution and consider its limitations when interpreting the obtained results. For example, anisotropic scattering rates or varying relaxation times across different states could significantly impact the accuracy of the results in some materials.

Another way to remove the iterative part of the BTE is to neglect the second term on the right-hand side of equation (10). This approach, which is usually referred to as the self-energy relaxation-time approximation (SERTA), is equivalent to ignoring the effects of backscattering $n\mathbf{k}$ (ref. 3). To approximately take the backscattering processes into account, one can add a geometrical factor to reduce the out-scattering rate. This leads to the so-called momentum relaxation-time approximation (MRTA), which will always give higher or equal mobility than the SERTA, by construction[2,12,13,35].

Finally, among the various other approximations, one noteworthy approach is the electron–phonon averaged (EPA) approximation[15,36]. This method relies on an energy-dependent averaging of phonon energies and a coarse-mesh treatment for the electron–phonon matrix elements. The EPA approximation has shown promising results when applied to the thermoelectric properties of half-Heusler compounds[36]. The `EPIC STAR`[37] code offers a related implementation of these ideas by employing a generalized Eliashberg function for short-range electron–phonon scattering, mirroring the methodology commonly applied in metallic systems. However, the long-range electron–phonon scattering is treated analytically in the same way as other first-principles approaches.

As the IBTE approach is now incorporated into many codes[13,15,20,38], it should be preferred over approximations. However, the CRTA, SERTA and MRTA are still frequently utilized, but caution is needed when employing them. It has been shown that the SERTA consistently underestimates the mobility, with extreme cases showing discrepancies of up to 70% (refs. 13,19,20). In the case of the MRTA, the analysis becomes more intricate. Generally, the MRTA results agree more closely with the IBTE solution compared with the SERTA, but significant deviations (more than 60%) have been observed in certain materials such as SrO, KH, $KMgH_3$, and MgO (ref. 13).

Figure 3 was computed using `ABINIT` for the purpose of this Review and depicts the variation in $\partial f/\partial E$ within the Brillouin zone of MgO for the two approximations and the IBTE approach. A clear movement of electrons in the opposite direction to the electric field is observed. Despite the similarities in the shapes of the areas across the various approximations, attributed to the use of similar electronic wavefunctions, there are notable distinctions in the $\partial f/\partial E$ values. For example, the most pronounced variation observed in the MRTA compared with the IBTE illustrates the substantial discrepancy observed in the mobility between the two methods. By contrast, the SERTA and IBTE mobilities are close in MgO owing to relatively similar $\partial f/\partial E$ values. Finally, the CRTA accuracy heavily relies on the choice of the lifetime. Numerous studies have reported reasonably good results when using lifetimes ranging from 10^{-14} s to 10^{-15} s (ref. 29). However, it is essential to acknowledge that the CRTA does not demonstrate high overall accuracy, even concerning material ranking[13]. Calculating the Seebeck coefficient is an exception here as high and low Seebeck materials can be directly estimated using the CRTA as this quantity depends less on relaxation time[29,34].

Interpolation schemes, dipoles and quadrupoles. Nowadays, the majority of cutting-edge codes designed for the computation of electron–phonon quantities using first-principles methodologies offer the option to employ either the iterative approach or approximations[13,15,20,38]. The differences between these codes lies in their strategies for acquiring these electron–phonon quantities and the specific interpolation techniques they employ. In fact, the main problem in obtaining accurate electron–phonon mobilities is the need to obtain matrix elements from density functional perturbation theory (DFPT) on very dense $\mathbf{k}$-point and $\mathbf{q}$-point grids. One way to reduce the computational cost is to interpolate the electron–phonon matrix elements using Fourier transforms. For example, `EPW`[20], `PERTURBO`[38] and `PHOEBE`[15] rely on an interpolation framework that exploits the spatial localization of Wannier functions in real space, facilitating the calculation of electron–phonon matrix elements at relatively economical computational expense. These maximally localized Wannier functions

are constructed using the Wannier90 code[39,40]. However, despite substantial recent advancements[41–44], the generation of these maximally localized Wannier functions remains intricate and time-intensive for systems that are more difficult to interpret in terms of chemical orbitals, which poses challenges to the automation of material database computations.

Recently, a new Wannier-based approach, leveraging the compression of electron–phonon interactions, has achieved a substantial speed-up in the computation of electron–phonon matrices without compromising accuracy[45]. This data-driven methodology reveals that current first-principles calculations might overparameterize the electron–phonon interaction, and such complexity may be unnecessary to achieve state-of-the-art results. By contrast, the ABINIT[46,47] software adopts an alternative strategy based on the direct interpolation of the perturbed potential. This approach offers the advantage of circumventing the need for Wannier functions, but demands more memory and time compared with Wannier-based approaches. Nevertheless, through the implementation of various optimization techniques[6], this approach has recently enabled first-principles medium-throughput explorations of mobility[13].

For the interpolation, the short-range interactions pose no major challenge, as these contributions rapidly approach zero beyond the boundaries of the real-space box. By contrast, handling long-range interactions in semiconductors by interpolation is more intricate, as they can produce non-analytical solutions as $\mathbf{q}$ approaches zero. In such cases, Fourier interpolation is inadequate, and specific analytical models must be employed to address these interactions, such as the dipole interaction prevalent in polar materials[48–51]. Recently, the significance of incorporating dynamical quadrupoles has emerged as a crucial factor for achieving accurate transport results[6,11,52,53]. Importantly, when using a Wannier interpolation-based scheme, a Berry connection term appears at the same second order as dynamical quadrupoles and has been shown to be of similar importance[54,55]. In contrast to dipoles, which are only present in polar materials, dynamical quadrupoles are non-zero in all noncentrosymmetric crystals, but also in centrosymmetric ones if one or more atoms are placed at noncentrosymmetric sites, which make dynamical quadrupoles important for the computation of transport properties in many materials[6,11,19,52,53,55]. Finally, we mention that in 2D materials the long-range electrostatics has to be treated carefully[54–56] and used in conjunction with out-of-plane truncation schemes[57].

Empirical models. Although recent efforts have shown automation of transport computations using the full electron–phonon information, the computational resources needed have restricted screening studies to relatively small number of materials with a limited number of atoms. Consequently, alternative approaches that would be amenable to high-throughput computing have garnered attention in the scientific community. Among these, empirical models have emerged as a prominent choice, facilitating rapid calculations albeit at the expense of the accuracy of fully first-principles methods. Empirical and semi-empirical models, for example, for lifetimes calculations, have been formulated and implemented since the early 1930s[1,58–60] and still provide the basis of model-based contemporary approaches. Usually, the different scattering interactions are split into different models that depend on specific parameters, which can be obtained from experiments or theory. For example, ref. 58 described the coupling between polar optical phonons and electrons in polar materials, the so-called Fröhlich interaction, based on the isotropic dielectric constants and the longitudinal optical frequency. Subsequently, ref. 61 extended this model to include the anisotropy of dielectric constants and involving multiple longitudinal optical modes. This extended version is still used today, either directly[62,63] or as a foundational framework[64,65].

Recently, a model-based software called AMSET[12] has allowed to efficiently calculate anisotropic transport properties using first-principles data, marking a notable advancement. This approach enables the computation of anisotropic acoustic deformation potentials, piezoelectric, ionized impurity and polar electron–phonon scatterings. AMSET uses models at the level of the electron–phonon matrix elements as this stage remains the main bottleneck in the BTE framework in terms of computational resources. AMSET supports anisotropic materials, relies on routinely available inputs and is mostly based on the MRTA. However, the polar electron–phonon coupling is treated with the SERTA and, as discussed previously, this approximation is frequently associated with significant underestimations compared with the IBTE solution[13,19,20]. This discrepancy can pose challenges when dealing with materials in which the polar electron–phonon coupling is important, as exemplified recently in the case of CuI[66].

Nevertheless, AMSET has proven to be a useful methodology for efficiently computing large material databases at lower computational cost. It offers an average speed-up of four orders of magnitude compared with DFPT methods for computing transport properties[12] and at the same time consistently demonstrates strong agreement with experimental results. Notably, recent efforts have harnessed AMSET for high-throughput computational tasks, leveraging machine learning to generate inputs used in the AMSET models across a data set spanning over more than 20,000 materials[67].

Kubo formalism

The BTE approach offers an effective framework for handling time-independent electric fields but it relies strongly on DFPT and typically ignores higher-order electron–phonon interactions. As an alternative, the Kubo formalism[68,69] can be used to compute transport coefficients. Kubo approaches are more often used for computing thermal properties, such as thermal conductivities[70,71], but can also be implemented for electronic transport.

For homogeneous systems, the optical conductivity tensor linearly connects the macroscopic current density $\mathbf{J}$ and the applied external electric field $\mathbf{E}$:

$$\sigma_{\alpha\beta}(t,t') = \frac{1}{V}\int \mathrm{d}^3 r \left.\frac{\partial J_\alpha(\mathbf{r},t)}{\partial E_\beta(t')}\right|_{\mathbf{E}=\mathbf{0}}, \tag{17}$$

in which the current density can be expressed as correlation functions, which only depend on time differences and allow for a convenient Fourier transform[2,72–74]

$$\sigma_{\alpha\beta}(\omega) = i\frac{e^2}{m_e\omega}\delta_{\alpha\beta}n^{\mathrm{el}} + \frac{1}{\hbar\omega V}\iint \mathrm{d}^3 r \mathrm{d}^3 r' \mathcal{I}^{\mathrm{p}}_{\alpha\beta}(\mathbf{r},\mathbf{r}',\omega), \tag{18}$$

in which the first term stems from the equilibrium charge density of n^{el} electrons and the second is the retarded paramagnetic contribution to the current density. The remaining contribution is a diamagnetic one and is null in the Coulomb gauge, used here. We see that equation (18) is insightful because it relates current fluctuations in thermal equilibrium (first term on the right-hand side of the equation) to the electrical conductivity, which is a non-equilibrium dissipation property. This connection between non-equilibrium and equilibrium quantities is at the heart of the fluctuation-dissipation theorem on which the Kubo formula is built[75].

To solve equation (18) in practice, one often uses the independent-particle approximation (IPA) in which the two-particle correlation function is approximated by the product of two one-particle correlation functions. The strongly correlated electrons community also calls this the Kubo optical conductivity without current vertex correction[76]. It is comparable to the SERTA approximation within the BTE for time-independent electric fields. The independent-particle approximation leads to an expression involving the one-particle Green's function that can be written in terms of the electronic spectral function $A_{n\mathbf{k}}(\omega)$, finally giving the practical formula:

$$\sigma_{\alpha\beta}^{\mathrm{IPA}}(\omega) = i\frac{e^2}{m_e\omega}\delta_{\alpha\beta}n^{\mathrm{el}} + i\frac{e^2}{V}\sum_{mn}\int\frac{\mathrm{d}^3k}{\Omega^{\mathrm{BZ}}}v_{mn\alpha\mathbf{k}}v_{nm\beta\mathbf{k}}\iint \mathrm{d}\omega'\mathrm{d}\omega'' \frac{f(\hbar\omega'') - f(\hbar\omega')}{\hbar\omega}\frac{A_{n\mathbf{k}}(\omega')A_{m\mathbf{k}}(\omega'')}{\omega + \omega'' - \omega' + i\eta}, \quad (19)$$

in which $f(\hbar\omega)$ are the electronic occupation functions. We refer the interested reader to Appendices B and C of ref. 2 for a discussion of the separation of the current density into diamagnetic and paramagnetic contributions and for the derivation of the IPA.

The Kubo formula in the IPA, equation (19), can be approximated even further by replacing the spectral functions by the quasiparticle eigenvalues, which gives the Kubo–Greenwood (KG) formula[68,77–79]:

$$\sigma_{\alpha\beta}^{\mathrm{KG}}(\omega) = \frac{2\pi e^2\hbar}{3Vm_e^2\omega}\sum_{mn}\int\frac{\mathrm{d}^3k}{\Omega^{\mathrm{BZ}}}v_{mn\alpha\mathbf{k}}v_{nm\beta\mathbf{k}}(f_{n\mathbf{k}}^0 - f_{m\mathbf{k}}^0)\times\delta(\varepsilon_{m\mathbf{k}} - \varepsilon_{n\mathbf{k}} - \hbar\omega), \quad (20)$$

in which, regardless of the level of approximation, the optical conductivity must always satisfy the integration sum rule $\frac{2m_eV}{3\pi e^2}\sum_\alpha\int_0^\infty\sigma_{\alpha\alpha}(\omega)\mathrm{d}\omega = 1$ (ref. 72).

Note that equation (20) is temperature-independent and does not include any phonon dependence beyond the small electronic temperature contribution from the electronic occupation. Instead, equation (19) has an additional temperature-dependent contribution coming from the electronic spectral function $A_{n\mathbf{k}}(\omega, T)$, which can include electron–phonon[80] but also electron–electron[81,82] corrections.

Temperature and phonon effects can be taken into account by averaging σ^{KG} over an uncorrelated atomic configuration generated from ab initio molecular dynamics simulation in the NVT canonical ensemble at finite temperature using supercells[83,84]. We note that this approach combining ab initio molecular dynamics and the KG formalism naturally accounts for electron–phonon interactions and anharmonicity. It can also be implemented on any functional without the lengthy developments needed to implement DFPT on new functionals. The KG approach was used to study the optical and DC electric conductivity of aluminium[78], dense helium[85] and bcc iron[86]. `ABINIT` allows KG simulations[87], and the temperature-independent KG conductivity is implemented in the `KGEC` code within a projector-augmented wave basis set[88]. By taking snapshots of ab initio molecular dynamics simulations, transport results were obtained for $Cu_{12}Sb_4S_{13}$ as a function of temperature[89], with results about two times larger than experimental values. More recently, temperature has been included in the `FHI-kubo`[84] and `FHI-vibes`[90] codes. However, the conductivity of silicon obtained by KG underestimates both BTE and experimental results by about 50%.

It is worth mentioning that mirroring the ultra-dense momentum sampling for BTE, the ab initio molecular dynamics approach suffers convergence challenges with increasing supercell size, but it can be advantageous when dealing with strongly anharmonic materials[84]. Finally, interesting results have been obtained with `LinReTrace`, mostly in narrow-gap semiconductors, using a semi-analytical evaluation of the Kubo formula for the resistivity but also for Seebeck, Nernst and Hall coefficients[74,91].

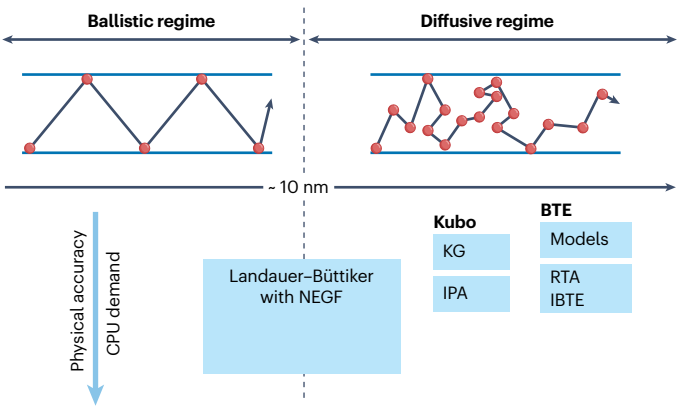

Fig. 4 | Schematic representation of diffusive and ballistic transport. Different theoretical frameworks can be used in the two regimes, which are characterized by their accuracy and computational demand. The methods include the Landauer–Büttiker formalism with non-equilibrium Green's function (NEGF), the Kubo formalism, the Kubo–Greenwood (KG) formula, the independent-particle approximation (IPA), as well as the Boltzmann transport equation (BTE), relaxation-time approximations (RTAs) and iterative Boltzmann transport equation (IBTE).

Landauer–Büttiker formalism

Although the BTE remains the preferred formalism for bulk semiconductors in the classical diffusion regime, in which the mean-free path of the carriers is smaller than the device size, alternative approaches become necessary as the system size diminishes, as shown in Fig. 4. If the mean-free path of the carriers (λ) becomes longer than the device, the system can be described ballistically, and the Landauer framework becomes useful. In this approach, the transport is treated as a flow of electrons between two reservoirs separated by a scattering region[92] (Fig. 5). This method is often called the Landauer–Büttiker approach after Markus Büttiker extended it to many-terminal systems or probes that can model the different scattering processes[93,94]. The Landauer–Büttiker approach is frequently employed to evaluate carrier transport in mesoscopic structures operating at low temperatures[95,96], especially for thermoelectric materials, but it also finds many applications for lower-dimensional materials. For example, in the 1D case, the mean-free path of a carrier between two scattering events becomes bigger than the sample dimension, which makes ballistic transport[97–100] a valid approach. Its applicability can also extend to higher temperature regimes, offering a more intuitive perspective on transport phenomena[101–103].

In the same way as the BTE, the transport parameters under the Landauer–Büttiker approach show a direct correlation with the electronic band structure of the material. Fundamental transport quantities such as the electrical conductivity σ, the Seebeck coefficient S and the electronic component of thermal conductivity κ_e can be expressed as

$$\sigma = \left(\frac{2e^2}{h}\right) I_0,$$
$$S = -\left(\frac{k_B}{e}\right)\frac{I_1}{I_0}, \quad (21)$$
$$\kappa_e = \frac{2k_B^2 T}{h}\left(I_2 - \frac{I_1^2}{I_0}\right),$$

with the current I described by

$$I_j = \int_{-\infty}^{\infty} \bar{T}(E)\left(\frac{E-\mu}{k_B T}\right)^j \frac{-\partial f^0}{\partial E} dE. \quad (22)$$

The current I expresses the change in the Fermi–Dirac distribution function f^0 between two reservoirs separated by a region of scattering as shown in Fig. 5. In this expression, μ is the Fermi level and $\bar{T}(E) = T(E)M(E)$ represents the transmission with $M(E)$ the distribution of modes which corresponds to the number of conductive channels available for transport[95,97,98,102]. In the case of purely ballistic conduction, which is free from scattering, the transmission is equal to one. In the presence of scattering events, the transmission is often replaced by the transport distribution $\Sigma(E)$ as defined by

$$\Sigma(E) = \frac{1}{\Omega}\sum_k v_x^2(k)\tau(k)\delta(E-\varepsilon_k), \quad (23)$$

in which similarities with the BTE are observed; ε_k is the band structure, $\tau(k)$ the scattering time and $v_x^2(k)$ the group velocity in the direction of transport (here the $\hat{x}$). $\Sigma(E)$ is often re-arranged to produce a more physically intuitive expression related to two parameters — the distribution of modes $M(E)$ and the mean-free path for backscattering $\lambda(E)$, the average distance along the transport direction before a change of sign of the electron velocity owing to the scattering ($\lambda \simeq v\tau$), in such a manner that

$$\Sigma(E) = \frac{2}{h}M(E)\lambda(E), \quad (24)$$

and therefore the Landauer–Büttiker results agree with the BTE within the RTA. In fact, $M(E)$ in the Landauer–Büttiker formalism is analogous to the conductivity effective mass in the Boltzmann approach[102]. Whereas $M(E)$ and v_x are directly linked to the band structure of the material, the lifetime τ in equation (23) (or equivalently the mean-free path λ in equation (24)) depends on different scattering mechanisms. In the same way as BTE, τ can be computed accurately using DFT-based methods. However, it is often approximated using simplified scattering models, such as assuming a constant τ (or $\lambda(E)$), or employing a model based on the density of states, as a higher density of states leads to more scattering possibilities[98,100,102].

This formalism has been implemented in several software packages, starting with the `PWCOND` code within `Quantum ESPRESSO` in the early 2000s, which mainly follow the work of refs. 104,105. Most often, the Landauer–Büttiker framework is used as a post-processing tool of the non-equilibrium Green's function (NEGF) approach[106]. The NEGF methods describe many-body ab initio approaches, which solve the general Kadanoff–Baym equations of motion[107]. In the context of the Landauer–Büttiker transport framework, the NEGF is used to compute the transmission function that provides various transport properties. Although the practical theory to include phonon contributions has been formally derived[106], we are not aware of any implementation.

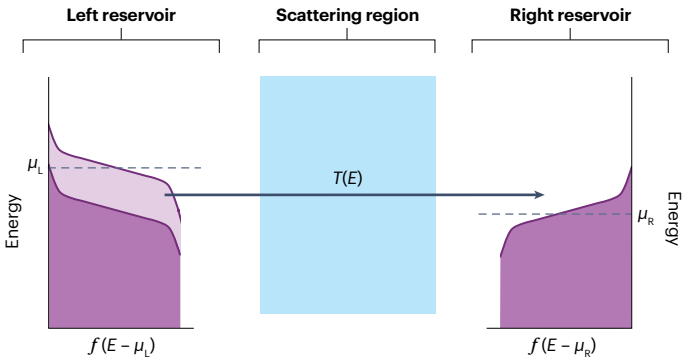

Fig. 5 | Schematic representation of the Landauer–Büttiker theory. Transport is determined by a transmission function $T(E)$ between two reservoirs characterized by different Fermi levels μ_L and μ_R and thus different distribution functions $f(E-\mu)$, E being the energy.

Many ab initio codes based on the Landauer–Buttiker and NEGF have been developed to compute transport phenomena, including `TRANSIESTA`[108], `Inelastica`[109–112], `ATK`[113], `NanoDCAL`[114,115], `Questaal`[116], `nextnano.NEGF`[117] or `ONETEP`[118,119]. Alternatively, NEGF can also be used to compute transport properties based on other frameworks such as the dR/dL[120] method in the `OMEN` code[121–123].

Given that the implementation of NEGF is in real space, these codes almost always rely on a localized basis set with a local Hamiltonian and a local Green's function. A recent work[124] used a plane wave basis set with wavefunction matching to satisfy open boundary conditions to perform large-scale NEGF simulation. Alternatively, a connection between plane-wave codes and localized basis sets can be obtained via Wannier functions, and this is the approach followed by the `WanT` code[125].

Comparison of the different frameworks

Over the past decades, the theoretical description of electronic transport in solids has predominantly relied on the BTE. With the iterative solution of the BTE now implemented in most codes, this method offers a good balance between accuracy and computational cost for systems of limited size. Overall, the mobilities computed using the BTE are in close agreement with experimental data[2,19], typically falling within the upper range of experimental values or slightly overestimating them. This overestimation is expected because the calculations only consider phonon scattering, whereas experiments can have additional scattering channels, such as impurities. For the approximations used in the BTE, it has been shown that the SERTA tends to underestimate the exact IBTE result, whereas the discrepancies observed with the MRTA are more system-dependent[13]. Figure 6 presents calculated mobility values based on the BTE, KG and NEGF methods and compares them with experimental measurements for Si and n-type MoS_2. For Si, the different RTA approximations (primarily the SERTA and the MRTA) closely match the IBTE solution[35,126]. By contrast, the spread in the RTA values is more pronounced for n-type MoS_2, with the MRTA values generally higher than those obtained with the SERTA. Beyond the effect of different approximations, the wide range of values from the IBTE results indicates how transport computations depend on the specific parameter of the computations (for example, the functional used or the convergence criteria). In addition, the BTE is still limited to relatively small unit cells — the currently largest system comprising nearly 80 atoms in the unit cell[127]. To address the computational bottleneck posed by DFPT electron–phonon matrix elements

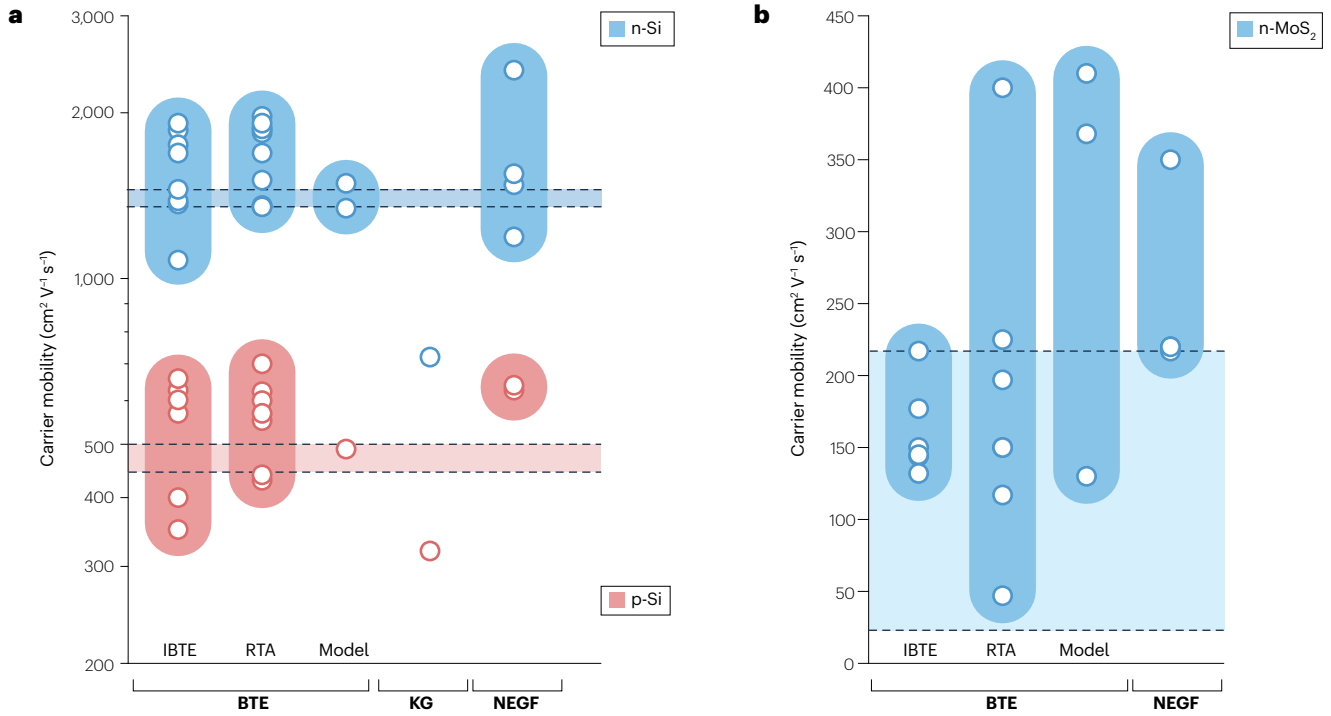

Fig. 6 | Calculated values of carrier mobility at room temperature using different frameworks and methods. a, Bulk p-type and n-type Si (in red and blue, respectively). **b**, Bulk n-type MoS_2. The shaded region corresponds to experimental measurements. For Si, the electron mobilities are from refs. 3,14,19,35,123,126,238 (iterative Boltzmann transport equation, IBTE), refs. 3,6,19,35,126,238,239 (self-energy relaxation-time approximation, SERTA), refs. 35,126 (momentum relaxation-time approximation, MRTA), refs. 12,240 (Boltzmann transport equation, BTE-based models), ref. 84 (Kubo–Greenwood, KG), refs. 113,238,241 (non-equilibrium Green's function, NEGF) and refs. 242–244 (experimental results). The hole mobilities are from refs. 3,19,126,238 (IBTE), refs. 3,19,126,238 (SERTA), ref. 126 (MRTA), ref. 245 (BTE-based models), ref. 84 (KG), ref. 238 (NEGF) and refs. 242,244 (experimental results). For MoS_2, the electron mobilities are from refs. 35,55,123,149,246,247 (IBTE), refs. 35,55,123,248,249 (SERTA), refs. 35,113 (MRTA), refs. 174,250,251 (BTE-based models), refs. 122,123,252 (NEGF) and refs. 173,253–255 (experimental results). The SERTA and MRTA results are grouped together under the term RTA.

in the BTE approach, the use of models provides a viable solution for handling larger systems with fairly good accuracy, particularly with the latest advancements in the AMSET software[12].

The Kubo framework has specific advantages over BTE. It does not have to rely on DFPT, which offers the possibility to treat anharmonicity, advanced functionals (hybrid or meta-generalized gradient approximation[128,129]) without major code implementation or strongly correlated systems[82]. However, the Kubo framework presents its own set of difficulties including the need for an accurate description of the spectral function and higher computational cost to integrate the additional frequency dimension. In practice, the Kubo formula is therefore often approximated by the KG equation. As explained previously, this method has been used to study the conductivity of metals, alloys and disordered materials[78,85,86]. Although it is possible to incorporate temperature effects by coupling the KG formula with ab initio molecular dynamics simulations, achieving fully ab initio temperature-dependent results for crystalline semiconductors remains challenging. In fact, these calculations are often prone to convergence issues related to the supercell size or require specific extrapolation methods[84,89]. As a result, KG-based studies on crystalline materials are rare, even for simple materials such as Si and show significant discrepancies with BTE and experiment as shown in Fig. 6.

Finally, the Landauer–Büttiker approach — either coupled with the NEGF method or not — is adequate for studying quantum transport in mesoscopic or low temperature systems but also for modelling full devices. However, bulk crystal results based on the Landauer–Büttiker formalism are uncommon. Figure 6 shows results obtained using the NEGF method for bulk silicon and MoS_2 based on either the Landauer–Büttiker approach or the dR/dL method. The use of NEGF provides computational result that aligns well with experimental findings, but it remains an expensive technique, with computational costs that scale approximately with the cube of the cross-section of the simulation channel[130]. The major advantages of the approach come from the possibility to combine phonon scattering with different scattering channels for mesoscopic systems.

Electron–phonon scattering in specific regimes

Following Fig. 1, we will now explore more specific regimes and their effect on transport. We will start with the effect of non-equilibrium phonons leading to drag effects. The transport in 2D and 1D will also be discussed before moving to the effects of high electric fields, spin–orbit coupling (SOC) and dielectric screening that can all significantly affect the electron–phonon coupling.

Phonon-drag and electron-drag effects

For electronic but also phonon transport within the Boltzmann transport formalism, a fundamental assumption — known as Bloch's assumption[131] — allows the complete separation of the electronic and

phononic BTEs. As a result, solving the BTE for electronic transport effectively reduces to considering the phonons to be in thermal equilibrium. Conversely, in thermal transport, the electronic system is assumed to be in equilibrium. This is what we consider to be a standard regime in Fig. 1. Clearly, each system should influence and interact with each other, and a momentum mixing between the electrons and the phonons should exist[132]. This momentum mixing was the starting point of a coupled theory of electron and phonon transport in solids in which the effect of non-equilibrium phonons is taken into account in electronic transport (phonon-drag effect) and vice versa (electron-drag effect).

By considering these effects in addition to the electric field **E** and temperature gradient, one can express the electron and phonon distribution function as[133,134]

$$f_{m\mathbf{k}} \approx f^0_{m\mathbf{k}}\left[1+(1-f^0_{m\mathbf{k}})\Psi_{m\mathbf{k}}\right], \tag{25}$$

$$n_{\mathbf{q}\nu} \approx n^0_{\mathbf{q}\nu}\left[1+(1+n^0_{\mathbf{q}\nu})\Phi_{\mathbf{q}\nu}\right], \tag{26}$$

with $\Psi_{m\mathbf{k}}$ and $\Phi_{\mathbf{q}\nu}$ the deviation functions related to the change from the electron and phonon equilibrium owing to an external field, respectively, and that can be described as

$$\Psi_{m\mathbf{k}} = -\beta\nabla T\cdot\mathbf{I}_{m\mathbf{k}} - \beta\mathbf{E}\cdot\mathbf{J}_{m\mathbf{k}}, \tag{27}$$

$$\Phi_{\mathbf{q}\nu} = -\beta\nabla T\cdot\mathbf{F}_{\mathbf{q}\nu} - \beta\mathbf{E}\cdot\mathbf{G}_{\mathbf{q}\nu}. \tag{28}$$

In these expressions, $\mathbf{I}_{m\mathbf{k}}$ and $\mathbf{F}_{\mathbf{q}\nu}$ stand for the electron and phonon response functions to an applied temperature gradient, respectively. In a similar way, $\mathbf{J}_{m\mathbf{k}}$ and $\mathbf{G}_{\mathbf{q}\nu}$ are the electron and phonon response functions to **E**. As response functions are related to each other due to the drag effects, this leads to a system of interdependent equations:

$$\mathbf{I} = \mathbf{I}^0 + \Delta\mathbf{I}^{\mathrm{S}}[\mathbf{I}] + \Delta\mathbf{I}^{\mathrm{D}}[\mathbf{F}], \tag{29}$$

$$\mathbf{F} = \mathbf{F}^0 + \Delta\mathbf{F}^{\mathrm{S}}[\mathbf{F}] + \Delta\mathbf{F}^{\mathrm{D}}[\mathbf{I}], \tag{30}$$

$$\mathbf{J} = \mathbf{J}^0 + \Delta\mathbf{J}^{\mathrm{S}}[\mathbf{J}] + \Delta\mathbf{J}^{\mathrm{D}}[\mathbf{G}], \tag{31}$$

$$\mathbf{G} = \underbrace{\mathbf{G}^0}_{=0} + \Delta\mathbf{G}^{\mathrm{S}}[\mathbf{G}] + \Delta\mathbf{G}^{\mathrm{D}}[\mathbf{J}], \tag{32}$$

in which terms with the superscript 0 represent the SERTA terms; those with the superscript S are the 'self' terms representing the in-scattering corrections, which are linked to the response function of the same species; and those with the superscript D are related to the 'drag' effects linked with the other species. It should be noted that the SERTA term for the phonon response to the electric field is null as **E** does not directly cause the diffusion of phonons. Usually, the SERTA term is calculated first (with the self and drag terms set to be zero) and then this feeds into the calculation of the two other terms through an iterative process until a convergence of the response functions[133–135]. We also note a recent extension to account for phonon coherence[136].

The impact of these drag effects on transport properties is quite diverse. When considering phonon drag as an electron travels across the lattice, its charge induces distortions or polarization in the nearby lattice, causing a loss of momentum in phonons. This, in turn, reduces the electron–phonon coupling, ultimately enhancing electronic transport. Conversely, electron drag leads to a decrease in electron momentum, resulting in reduced phonon momentum dissipation and thereby boosting thermal transport. In general, these effects therefore tend to improve transport properties. Overall, the effect of phonon drag on mobility at low carrier concentration seems negligible, and including drag effects leads to only small changes in mobility, for example, in Si[134,137], Si-C[135] and GaAs[133]. Similarly, the electron drag effect on phonon thermal conductivity is rather small[133–135,137].

However, the impact of drag effects is more important for the computation of the Seebeck coefficient, which directly depends on the drag effect when the flow of carriers and phonons is linked and no longer treated independently. In fact, the Seebeck coefficient can be divided into two parts: $S = S^{ED} + S^{D}$ in which 'ED' stands for the electron diffusion, which refers to the spatial variation of the electron distribution in the presence of a difference of temperature and 'D' for the new contribution from the drag effect between the lattice and the electrons[138,139]. Usually, the phonon-drag effect boosts the Seebeck coefficient, this increase being especially noticeable at lower temperatures, owing to the longer phonon mean-free path. This has been shown in $FeSb_2$ (ref. 139), Si[137,140], InSb[141] or GaN[142] with the phonon-drag effect, leading to an important enhancement of the Seebeck coefficient at low temperature.

In terms of implementation, options to compute the phonon-drag and electron-drag effects have emerged in existing transport codes. For example, a software package[143], built on a modified version of `EPW` to incorporate the drag effects and, initially used in a previous work[137], is now available. And recently, the coupled BTE solver `elphbolt` that uses data generated by external codes such as `EPW` and `Quantum ESPRESSO` has also been released[134].

Dimensionality effects: 2D and 1D

Low dimensionality materials, especially 2D materials, have been central to research on carrier transport since the first exfoliation of graphene[144] because of their emerging electronic properties[145,146]. It is therefore not surprising that they have also been at the centre of a number of theoretical studies. However, first-principles calculations based on plane-wave basis sets, such as the BTE, rely on 3D periodic boundary conditions. By contrast, simulating systems with a lower dimensionality introduce periodic images in non-periodic directions – specifically, one out-of-plane image in 2D and two out-of-chain images in 1D. In fact, the dimensionality of a material strongly influences its response to a long-wavelength periodic perturbation, which can lead to inaccuracies. Specifically, it may result in an erroneous depiction of long-wavelength electron-phonon dynamics, mainly in the treatment of polar Fröhlich and piezoelectric scattering[57,147,148]. It is therefore important to work in a more realistic framework that is adapted to these specificities[57,147].

In 2D, a first-principles framework based on DFPT and the BTE has been implemented[57]. Used for gate systems, it has recently allowed automatic computation of 2D materials[149] as well as high-throughput screening of large 2D database[147]. Lately, this framework has been extended to take into account the effect of dynamical quadrupoles in 2D materials, which are also essential to obtain accurate carrier mobility results[55]. Similarly, another 2D framework has been developed for low-dimensional interconnects while taking into account both electron–phonon and surface scatterings[150]. As in the 3D case, similar approximations have also been used to calculate the mobility in 2D materials such as SnSe, MXene or black phosphorus[151–153].

As mentioned previously, one can consider the 1D case as a ballistic problem and use the Landauer–Büttiker formalism to deal with this regime[148]. Lately, a DFPT framework with 1D open-boundary conditions has been implemented, allowing the effective response of such materials to be captured[154].

High electric field

In the presence of high electric fields, carriers within a semiconductor can amass a significant amount of energy, surpassing the average kinetic energy of the atomic lattice. Owing to this rapid gain of energy, which outpaces the rate at which they lose energy to the lattice, the carriers are no longer in thermal equilibrium. Having a higher temperature than the lattice, these carriers are usually labelled as warm carriers when $\Delta T/T_0 \ll 1$ and hot carriers when $\Delta T/T_0 \approx 1$ with ΔT the steady-state temperature rise of the carriers and T_0 the temperature of the lattice[22,155]. This phenomenon is commonly observed when Ohm's law becomes inadequate for describing electrical behaviour, which corresponds roughly to applied electric fields of 10^4 V cm^{-1} or more. In fact, for weaker fields, the drift velocity tends to increase linearly with the electric field. However, at higher fields, the increase becomes sublinear until the drift velocity saturates at ~10^7 cm s^{-1}. Whereas at low fields, carriers are mostly scattered by elastic processes involving momentum relaxation time and acoustic, piezoelectric or ionized impurity scattering, at high fields the inelastic interaction with optical phonons and inter-valley scattering becomes dominant, leading to the sublinear increase observed (and lower energy relaxation time). In certain n-type materials such as GaAs, InAs or AlN, a velocity overshoot — a maximum above the saturation velocity — can also be observed owing to secondary conduction band valleys that are close in energy to the CBM, which creates a competition between inter-valley and intra-valley relaxations[22,156]. Moreover, the prevailing transport theory, which traditionally assumes that electrons are predominantly scattered by a single phonon, fails to accurately describe the electron behaviour in high electric fields. In fact, this assumption has already been questioned at low field in materials such as GaAs[157] and Si[158], in which the incorporation of two-phonon processes leads to substantial alterations in mobility. In the case of high electric fields, the two-phonon scattering mechanism has been shown to influence both energy and momentum relaxation rates, as well as inter-valley scattering in GaAs[159].

Nevertheless, although electronic noise has been experimentally demonstrated[160,161], the study and understanding of these fluctuations in the context of non-equilibrium steady-state conditions lag behind the well-established treatments for low-field transport. In fact, mainly Monte-Carlo calculations with (semi)-empirical models have been used to treat these high-field phenomena[162–166]. But more recently, first-principles ab initio methods have begun to emerge by extending the BTE framework to address the specificities of the high-field case. For example, drift velocity curves have been obtained using the BTE in combination with full-band Monte-Carlo simulations[167]. Another option is time-stepping the BTE to steady state[168]. Finally, a new theory of electronic noise has been developed by Choi et al.[155] to treat warm electrons, which has been applied to GaAs with reasonable experimental agreement. A further extension of this methodology accounts for hot-carriers regimes[159,169].

High-κ dielectrics and remote phonon scattering

In most technological applications, such as microelectronics, carrier transport occurs in systems surrounded by dielectrics (characterized by a dielectric constant, κ). For a long time, silicon dioxide (SiO_2) has been the most widely used gate dielectric. However, as the scale of electronic devices kept decreasing, the thickness of the SiO_2 layer also had to be reduced to maintain similar device performance. This reduction exposed the device to significant leakage currents owing to quantum tunnelling effects, seriously threatening the reliability of SiO_2-based devices. To overcome this technical issue, materials with high dielectric constants (high-κ) were introduced to replace SiO_2, allowing increased dielectric thickness while maintaining the same capacitance[170].

From an application perspective, it is therefore important to consider the effect of dielectric screening on electron–phonon interactions and transport properties. For example, it has been shown both theoretically and experimentally that high-κ materials drastically reduce Coulombic impurity scattering, leading to higher mobility in semiconductors, close to the one limited by phonons only[171–174].

However, the use of high-κ dielectrics involves remote phonon scattering, which has been the object of a number of theoretical investigations. It originates from the interaction between the carriers inside the semiconductor and the hybrid excitation arising from the interaction of interface plasmons and optical phonons, impacting the transport[175–177]. This interaction between the carriers in the semiconductor and the surface-optical (SO) phonon modes of the dielectric can be described by a Fröhlich-like expression in which the coupling strength is proportional to

$$\left[\left(\frac{1}{\varepsilon_s^{\infty}+\varepsilon_d^{\infty}}-\frac{1}{\varepsilon_s^{\infty}+\varepsilon_d^{0}}\right)\hbar\omega_{SO}\right], \tag{33}$$

with the subscripts s and d denoting semiconductor and dielectric, respectively[175,177].

Remote phonon scattering is not dominant in SiO_2-based systems because of the rigid nature of the covalent Si–O bonds, which results in minimal ionic polarization and a weak coupling following equation (33). However, it becomes much more significant in high-κ dielectrics as they have a stronger ionic response compared with the low-κ SiO_2 (refs. 176–179). For instance, the use of high-κ dielectrics such as ZrO_2 or HfO_2 (which are widely used in the industry) on Si or Ge substrates tends to reduce the carrier mobility by half compared with similar system with SiO_2 owing to remote phonon scattering[180,181]. It is worth mentioning that the addition of a top gate dielectric can also mechanically quench homopolar phonons, as observed in MoS_2 (ref. 182). This could open new avenues for further mobility improvements by exploring different combinations of dielectric materials.

Spin

SOC can have a significant influence on the transport properties, particularly in p-type materials characterized by band degeneracy at the valence band minimum. In such materials, the degenerate bands are commonly referred to as the heavy-hole, light-hole and split-off bands, as illustrated in Fig. 7. Incorporating SOC into the analysis typically leads to the lifting of degeneracy among these bands, with the split-off band experiencing a decrease in energy. The resulting spin–orbit splitting can vary, ranging from relatively modest values such as −0.028 eV in Ge[183] and −0.044 eV in Si[184] to more substantial values such as −0.34 eV in GaAs[185] and −0.64 eV in CuI[186]. A substantial lift of degeneracy leads to an increase in the mobility as fewer scattering channels are present. In fact, the distribution of states that contribute to transport is situated very close to the upper edge of the valence band, typically peaking around $3/2k_BT$ from the band edge[146] and rapidly diminishing with

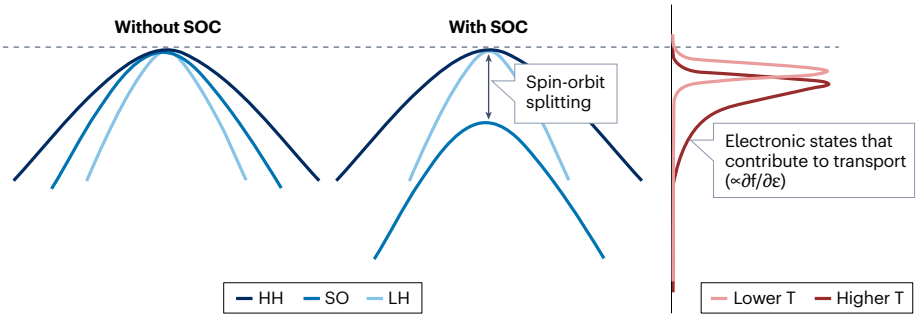

Fig. 7 | Schematic representation of the effect of spin–orbit coupling on three degenerate bands. The heavy hole (HH), split-off (SO) and light hole (LH) bands. In this schematic example, the SO band does no longer contribute to the transport after applying the spin–orbit coupling (SOC) because it moves away from the energies at which electrons take part in transport. This results in a reduction of the number of scattering channels and an increase of the mobility is expected.

increasing energy, as shown schematically in Fig. 7. Hence, when the splitting is significant enough, the split-off band can move beyond the energy range of states that actively participate in transport, resulting in the removal of this scattering channel. For example, in GaAs, the mobility is underestimated by ~50% when SOC is not considered[126], in CuI the difference is 37% (ref. 66) and it can reach 62% in AlSb owing to a computed spin–orbit splitting of 0.67 eV (ref. 19). In materials exhibiting a minor splitting, the underestimation at room temperature is considerably lower but still not negligible, with a difference of around 8% in the case of Si[3,126].

The concept of spin is directly related to another type of transport: spin transport, which relies on the ability of certain materials to generate and sustain a pure spin current. As our Review focuses on the transport of charge carriers, and spintronics represents a distinct area of research, we encourage readers to consult specific reviews on spin transport for a more in-depth exploration of this topic[187–190].

Strong electron–phonon coupling and polarons

When electron–phonon coupling becomes stronger, carriers become trapped within specific lattice sites, leading to a unique interplay between a self-localized carrier and the phonons that trap it — a quasiparticle called a polaron. Polaron transport is thought to have a crucial role in several materials including conducting oxides[191,192] and perovskites[193]. Polarons can be classified into two distinct categories: small polarons, confined within the length scale of the lattice constant, and large polarons, which extend across numerous unit cells.

Small polarons are present in the strong coupling regime and can only move through discrete hops from one lattice site to another. These hops are thermally activated, and in contrast to electrons or holes, small polarons follow an Arrhenius-like formula for mobility, where mobility increases with temperature. Overall, the mobility of small polarons remains low, typically below 0.1 $cm^2 V^{-1} s^{-1}$ (ref. 194). The computation of small polaron-hopping mobility can be achieved using models based on the Marcus[195] or Emin, Holstein, Austin and Mott theory[196–198]. In these approaches, the diffusion paths as well as the specific activation energy for the transition between the initial and final polaron states are commonly computed using the nudged elastic bands method[199–201] with DFT+U[202,203], or even hybrid functionals to avoid the typical overestimation of electron delocalization associated with semilocal functionals[204,205]. In addition, the hopping dynamics of small polarons can also be studied using molecular dynamics[206,207] or dynamical mean-field theory[208].

By contrast, the large polaron regime is characterized by an intermediate electron–phonon coupling strength, leading to a regime between the band-like and polaron-hopping limits. Large polarons maintain a moderate mobility and exhibit a transport behaviour more akin to that seen in band materials, with a mobility inversely proportional to the number of phonons[192,209–211]. In inorganic materials, the large polaron mobility can be obtained within the Boltzmann equation framework[212], using the Feynman, Hellwarth, Iddings and Platzman method[213–215] or more recently by using a finite-temperature cumulant approach coupled with a Kubo approach[80,216]. Finally, refs. 217,218 may enable possible polaron transport calculations using the primitive cell only, making it more computationally affordable.

Future developments

The field of electronic transport has made a giant leap in just a few decades. It moved from simple models of transport with parameters empirically fitted to experiment to the possibility to model entirely ab initio electron transport including phonon scattering. We expect a natural growth in the complexity of physical phenomena considered in transport studies as well as more routine use of first-principles electron transport computations for materials design.

One future development is the incorporation of temperature-dependent band structure renormalization in transport calculations[219–221]. In a similar way, the influence of thermal lattice expansion[3] and electron interaction with multiple phonons (anharmonicity)[157] should also lead to a more accurate picture of the transport phenomena in solids. These effects are not expected to have an important impact on the mobility of most of the materials but certain materials of great interest technologically (such as halide perovskites) might need those approaches to be treated accurately. Additionally, electron–phonon quantities are typically computed within DFPT and thus rely on semilocal functionals such as local-density approximation or generalized gradient approximation. Yet, certain materials require an extension beyond semilocal DFT to obtain accurate results. For example, small bandgap semiconductors or highly correlated oxides could be metallic within semilocal functionals making these functionals inadequate to study their transport. Adding a Hubbard U parameter has been a common way to correct these effects. Nevertheless, despite the development of DFPT+U formalisms[222,223], only few studies have used it to compute electron–phonon properties[82,224–226].

Addressing this challenge may also involve exploring alternative electron–phonon approaches such as finite differences calculations that allow the use of hybrid functionals or GW approximations based, for example, on the recent development of GW perturbation theory[227,228]. We note that the finite differences method might also be a promising way to incorporate electron–phonon terms beyond the first order, such as multiphonon terms. Despite significant advances in recent years, this method remains computationally demanding, particularly because of the requirement for large supercells, but we expect further developments that will help to alleviate the problem[227–229].

Alternative frameworks, such as KG, may be helpful here, but it will require tackling major challenges with convergence.

There has also been notable progress in extending first-principles transport computations to magnetic materials, but these theories are still limited to the 0K regime[230,231] or based on models for the description of magnetism[232–234]. With the importance of magnetic effects in areas such as spintronics, we also expect significant advances in this field in the coming years.

These theoretical developments will impact computational materials design, as transport is central to many applications from thermoelectrics to electronics. Efforts towards high throughput and databases have already emerged in the field and we anticipate that they will grow. These database efforts will enable the use of machine learning with various possible approaches. Machine learning has been impacting materials physics in the past few years and its use in transport and electron-phonon related properties is expected to grow[45,67,235,236].

Published online: 27 January 2025

References

1. Bloch, F. Über die quantenmechanik der elektronen in kristallgittern. *Zeitschrift für Physik* **52**, 555–600 (1929).
   First description of the electron–phonon interaction.
2. Poncé, S., Li, W., Reichardt, S. & Giustino, F. First-principles calculations of charge carrier mobility and conductivity in bulk semiconductors and two-dimensional materials. *Rep. Prog. Phys.* **83**, 036501 (2020).
   Important transport review including the derivations of the Boltzmann transport equation and Kubo.
3. Poncé, S., Margine, E. R. & Giustino, F. Towards predictive many-body calculations of phonon-limited carrier mobilities in semiconductors. *Phys. Rev. B* **97**, 121201 (2018).
4. Ziman, J. M. *Principles of the Theory of Solids* 2nd edn (Cambridge Univ. Press, 1972).
5. Blatt, F. J. in *Solid State Physics* Vol. 4, 199–366 (Elsevier, 1957).
6. Brunin, G. et al. Phonon-limited electron mobility in Si, GaAs, and GaP with exact treatment of dynamical quadrupoles. *Phys. Rev. B* **102**, 094308 (2020).
7. Giustino, F. Electron–phonon interactions from first principles. *Rev. Mod. Phys.* **89**, 015003 (2017).
8. Li, W., Carrete, J., Katcho, N. A. & Mingo, N. ShengBTE: a solver of the Boltzmann transport equation for phonons. *Comput. Phys. Commun.* **185**, 1747–1758 (2014).
9. Blöchl, P. E., Jepsen, O. & Andersen, O. K. Improved tetrahedron method for Brillouin-zone integrations. *Phys. Rev. B* **49**, 16223 (1994).
10. Lihm, J.-M., Poncé, S. & Park, C.-H. Self-consistent electron lifetimes for electron–phonon scattering. *Phys. Rev. B* **110**, L121106 (2024).
11. Brunin, G. et al. Electron–phonon beyond Fröhlich: dynamical quadrupoles in polar and covalent solids. *Phys. Rev. Lett.* **125**, 136601 (2020).
    Important work revealing the crucial importance of the quadrupolar interaction for the accurate computation of the mobility.
12. Ganose, A. M. et al. Efficient calculation of carrier scattering rates from first principles. *Nat. Commun.* **12**, 2222 (2021).
    Model-based Boltzmann transport equation approach that allows the efficient calculation of transport properties, paving the way for future high-throughput studies.
13. Claes, R., Brunin, G., Giantomassi, M., Rignanese, G.-M. & Hautier, G. Assessing the quality of relaxation-time approximations with fully automated computations of phonon-limited mobilities. *Phys. Rev. B* **106**, 094302 (2022).
    Comparison of the different approximations of the Boltzmann transport equation (BTE) as well as first medium-throughput computation of mobility based on the exact solution of the BTE.
14. Fiorentini, M. & Bonini, N. Thermoelectric coefficients of n-doped silicon from first principles via the solution of the Boltzmann transport equation. *Phys. Rev. B* **94**, 085204 (2016).
15. Cepellotti, A., Coulter, J., Johansson, A., Fedorova, N. S. & Kozinsky, B. Phoebe: a high-performance framework for solving phonon and electron Boltzmann transport equations. *J. Phys. Mater.* **5**, 035003 (2022).
16. Rode, D. in *Semiconductors and Semimetals* 1–89 (Elsevier, 1975); https://doi.org/10.1016/s0080-8784(08)60331-2.
17. Ghosh, K. & Singisetti, U. Rode's iterative calculation of surface optical phonon scattering limited electron mobility in n-polar GaN devices. *J. Appl. Phys.* **117**, 065703 (2015).
18. Macheda, F. & Bonini, N. Magnetotransport phenomena in p-doped diamond from first principles. *Phys. Rev. B* **98**, 201201 (2018).
19. Poncé, S. et al. First-principles predictions of Hall and drift mobilities in semiconductors. *Phys. Rev. Res.* **3**, 043022 (2021).
    Extension of the Boltzmann transport equation framework allowing the computation of the Hall mobility.
20. Lee, H. et al. Electron–phonon physics from first principles using the EPW code. *npj Comput. Mater.* **9**, 156 (2023).
21. Desai, D. C., Zviazhynski, B., Zhou, J.-J. & Bernardi, M. Magnetotransport in semiconductors and two-dimensional materials from first principles. *Phys. Rev. B* **103**, L161103 (2021).
22. Yu, P. Y. & Cardona, M. *Fundamentals of Semiconductors* (Springer, 2010); https://doi.org/10.1007/978-3-642-00710-1.
23. Madsen, G. K. H. & Singh, D. J. BoltzTraP. A code for calculating band-structure dependent quantities. *Comput. Phys. Commun.* **175**, 67–71 (2006).
24. Madsen, G. K. H., Carrete, J. & Verstraete, M. J. BoltzTraP2, a program for interpolating band structures and calculating semi-classical transport coefficients. *Comput. Phys. Commun.* **231**, 140–145 (2018).
25. Pizzi, G., Volja, D., Kozinsky, B., Fornari, M. & Marzari, N. BoltzWann: a code for the evaluation of thermoelectric and electronic transport properties with a maximally-localized Wannier functions basis. *Comput. Phys. Commun.* **185**, 422–429 (2014).
26. Smiadak, D. M. et al. Quasi-1D electronic transport and isotropic phonon transport in the Zintl $Ca_5In_2Sb_6$. *Mater. Today Phys.* **22**, 100597 (2022).
27. Chmielowski, R. et al. Theoretical and experimental investigations of the thermoelectric properties of Bi_2S_3. *J. Appl. Phys.* **117**, 125103 (2015).
28. Hautier, G., Miglio, A., Ceder, G., Rignanese, G.-M. & Gonze, X. Identification and design principles of low hole effective mass p-type transparent conducting oxides. *Nat. Commun.* **4**, 1–7 (2013).
29. Ricci, F. et al. An ab initio electronic transport database for inorganic materials. *Sci. Data* **4**, 1–13 (2017).
30. Ricci, F., Dunn, A., Jain, A., Rignanese, G.-M. & Hautier, G. Gapped metals as thermoelectric materials revealed by high-throughput screening. *J. Mater. Chem. A* **8**, 17579–17594 (2020).
31. Faghaninia, A. et al. A computational assessment of the electronic, thermoelectric, and defect properties of bournonite ($CuPbSbS_3$) and related substitutions. *Phys. Chem. Chem. Phys.* **19**, 6743–6756 (2017).
32. Brunin, G., Ricci, F., Ha, V.-A., Rignanese, G.-M. & Hautier, G. Transparent conducting materials discovery using high-throughput computing. *npj Comput. Mater.* **5**, 1–13 (2019).
33. Gibbs, Z. M. et al. Effective mass and Fermi surface complexity factor from ab initio band structure calculations. *npj Comput. Mater.* **3**, 1–7 (2017).
34. Chen, W. et al. Understanding thermoelectric properties from high-throughput calculations: trends, insights, and comparisons with experiment. *J. Mater. Chem. C* **4**, 4414–4426 (2016).
35. Li, W. Electrical transport limited by electron–phonon coupling from Boltzmann transport equation: an ab initio study of Si, Al, and MoS_2. *Phys. Rev. B* **92**, 075405 (2015).
36. Samsonidze, G. & Kozinsky, B. Accelerated screening of thermoelectric materials by first-principles computations of electron–phonon scattering. *Adv. Energy Mater.* **8**, 1800246 (2018).
37. Deng, T. et al. EPIC STAR: a reliable and efficient approach for phonon- and impurity-limited charge transport calculations. *npj Comput. Mater.* **6**, 46 (2020).
38. Zhou, J.-J. et al. Perturbo: a software package for ab initio electron–phonon interactions, charge transport and ultrafast dynamics. *Comput. Phys. Commun.* **264**, 107970 (2021).
39. Mostofi, A. A. et al. wannier90: a tool for obtaining maximally-localised Wannier functions. *Comput. Phys. Commun.* **178**, 685–699 (2008).
40. Pizzi, G. et al. Wannier90 as a community code: new features and applications. *J. Phys. Condens. Matter.* **32**, 165902 (2020).
41. Damle, A., Lin, L. & Ying, L. SCDM-k: localized orbitals for solids via selected columns of the density matrix. *J. Comput. Phys.* **334**, 1–15 (2017).
42. Vitale, V. et al. Automated high-throughput Wannierisation. *npj Comput. Mater.* **6**, 66 (2020).
43. Qiao, J., Pizzi, G. & Marzari, N. Projectability disentanglement for accurate and automated electronic-structure Hamiltonian. *npj Comput. Mater.* **9**, 208 (2023).
44. Qiao, J., Pizzi, G. & Marzari, N. Automated mixing of maximally localized Wannier functions into target manifolds. *npj Comput. Mater.* **9**, 206 (2023).
45. Luo, Y., Desai, D., Chang, B. K., Park, J. & Bernardi, M. Data-driven compression of electron–phonon interactions. *Phys. Rev. X* **14**, 021023 (2024).
46. Romero, A. H. et al. ABINIT: overview and focus on selected capabilities. *J. Chem. Phys.* **152**, 124102 (2020).
47. Gonze, X. et al. The ABINIT project: impact, environment and recent developments. *Comput. Phys. Commun.* **248**, 107042 (2020).
48. Gonze, X. & Lee, C. Dynamical matrices, born effective charges, dielectric permittivity tensors, and interatomic force constants from density-functional perturbation theory. *Phys. Rev. B* **55**, 10355–10368 (1997).
49. Verdi, C. & Giustino, F. Fröhlich electron–phonon vertex from first principles. *Phys. Rev. Lett.* **115**, 176401 (2015).
50. Zhou, J.-J. & Bernardi, M. Ab initio electron mobility and polar phonon scattering in GaAs. *Phys. Rev. B* **94**, 201201 (2016).
51. Sjakste, J., Vast, N., Calandra, M. & Mauri, F. Wannier interpolation of the electron–phonon matrix elements in polar semiconductors: polar-optical coupling in GaAs. *Phys. Rev. B* **92**, 054307 (2015).
52. Jhalani, V. A., Zhou, J.-J., Park, J., Dreyer, C. E. & Bernardi, M. Piezoelectric electron–phonon interaction from ab initio dynamical quadrupoles: impact on charge transport in wurtzite GaN. *Phys. Rev. Lett.* **125**, 136602 (2020).
53. Park, J., Zhou, J.-J., Jhalani, V. A., Dreyer, C. E. & Bernardi, M. Long-range quadrupole electron–phonon interaction from first principles. *Phys. Rev. B* **102**, 125203 (2020).
    Important work revealing the crucial importance of the quadrupolar interaction for the accurate computation of the mobility.

54. Poncé, S., Royo, M., Gibertini, M., Marzari, N. & Stengel, M. Accurate prediction of Hall mobilities in two-dimensional materials through gauge-covariant quadrupolar contributions. *Phys. Rev. Lett.* **130**, 166301 (2023).
55. Poncé, S., Royo, M., Stengel, M., Marzari, N. & Gibertini, M. Long-range electrostatic contribution to electron–phonon couplings and mobilities of two-dimensional and bulk materials. *Phys. Rev. B* **107**, 155424 (2023).
56. Royo, M. & Stengel, M. Exact long-range dielectric screening and interatomic force constants in quasi-two-dimensional crystals. *Phys. Rev. X* **11**, 041027 (2021).
57. Sohier, T., Calandra, M. & Mauri, F. Density functional perturbation theory for gated two-dimensional heterostructures: theoretical developments and application to flexural phonons in graphene. *Phys. Rev. B* **96**, 075448 (2017).
Extension of the density functional perturbation theory (and Boltzmann transport equation) for 2D materials.
58. Fröhlich, H. Electrons in lattice fields. *Adv. Phys.* **3**, 325–361 (1954).
59. Harrison, W. A. Scattering of electrons by lattice vibrations in nonpolar crystals. *Phys. Rev.* **104**, 1281–1290 (1956).
60. Herring, C. & Vogt, E. Transport and deformation-potential theory for many-valley semiconductors with anisotropic scattering. *Phys. Rev.* **101**, 944–961 (1956).
61. Vogl, P. Microscopic theory of electron–phonon interaction in insulators or semiconductors. *Phys. Rev. B* **13**, 694–704 (1976).
62. Hu, Y. et al. First principles calculations of intrinsic mobilities in tin-based oxide semiconductors SnO, SnO_2, and Ta_2SnO_6. *J. Appl. Phys.* **126**, 185701 (2019).
63. Hu, Y., Yao, X., Schlom, D. G., Datta, S. & Cho, K. First principles design of high hole mobility p-type Sn–O–X ternary oxides: valence orbital engineering of Sn^{2+} in Sn^{2+}–O–X by selection of appropriate elements X. *Chem. Mater.* **33**, 212–225 (2020).
64. Schlipf, M., Poncé, S. & Giustino, F. Carrier lifetimes and polaronic mass enhancement in the hybrid halide perovskite $CH_3NH_3PbI_3$ from multiphonon Fröhlich coupling. *Phys. Rev. Lett.* **121**, 086402 (2018).
65. Guster, B. et al. Fröhlich polaron effective mass and localization length in cubic materials: degenerate and anisotropic electronic bands. *Phys. Rev. B* **104**, 235123 (2021).
66. Willis, J. et al. Limits to hole mobility and doping in copper iodide. *Chem. Mater.* **35**, 8995–9006 (2023).
67. Ganose, A. M., Park, J. & Jain, A. The temperature-dependence of carrier mobility is not a reliable indicator of the dominant scattering mechanism. Preprint at https://arxiv.org/abs/2210.01746 (2022).
68. Kubo, R. Statistical–mechanical theory of irreversible processes. I. General theory and simple applications to magnetic and conduction problems. *J. Phys. Soc. Jpn.* **12**, 570–586 (1957).
First description of the general Kubo theory use for transport calculation.
69. Kubo, R. The fluctuation-dissipation theorem. *Rep. Prog. Phys.* **29**, 255 (1966).
70. Carbogno, C., Ramprasad, R. & Scheffler, M. Ab initio Green–Kubo approach for the thermal conductivity of solids. *Phys. Rev. Lett.* **118**, 175901 (2017).
71. Knoop, F., Scheffler, M. & Carbogno, C. Ab initio Green–Kubo simulations of heat transport in solids: method and implementation. *Phys. Rev. B* **107**, 224304 (2023).
72. Mahan, G. D. *Many-Particle Physics* (Springer, 2000); https://doi.org/10.1007/978-1-4757-5714-9.
73. Tomczak, J. M. *Propriétés spectrales et optiques des Matériaux corrélés*. Thesis, Ecole Polytechnique X. (2007); https://pastel.hal.science/pastel-00003163.
74. Pickem, M., Maggio, E. & Tomczak, J. M. LinReTraCe: the linear response transport centre. *SciPost Physics Codebases* https://doi.org/10.21468/SciPostPhysCodeb.16 (2023).
75. Kubo, R. Brownian motion and nonequilibrium statistical mechanics. *Science* **233**, 330–334 (1986).
76. Kim, S., Woo, S. & Min, H. Vertex corrections to the dc conductivity in anisotropic multiband systems. *Phys. Rev. B* **99**, 165107 (2019).
77. Greenwood, D. A. The Boltzmann equation in the theory of electrical conduction in metals. *Proc. Phys. Soc.* **71**, 585–596 (1958).
78. Desjarlais, M. P., Kress, J. D. & Collins, L. A. Electrical conductivity for warm, dense aluminum plasmas and liquids. *Phys. Rev. E* **66**, 025401 (2002).
79. Holst, B., French, M. & Redmer, R. Electronic transport coefficients from ab initio simulations and application to dense liquid hydrogen. *Phys. Rev. B* **83**, 235120 (2011).
80. Zhou, J.-J. & Bernardi, M. Predicting charge transport in the presence of polarons: the beyond-quasiparticle regime in $SrTiO_3$. *Phys. Rev. Res.* **1**, 033138 (2019).
81. Sihi, A. & Pandey, S. K. TRACK: a Python code for calculating the transport properties of correlated electron systems using Kubo formalism. *Comput. Phys. Commun.* **285**, 108640 (2023).
82. Abramovitch, D. J., Zhou, J.-J., Mravlje, J., Georges, A. & Bernardi, M. Combining electron–phonon and dynamical mean-field theory calculations of correlated materials: transport in the correlated metal Sr_2RuO_4. *Phys. Rev. Mater.* **7**, 093801 (2023).
83. Chen, A.-B., Weisz, G. & Sher, A. Temperature dependence of the electron density of states and dc electrical resistivity of disordered binary alloys. *Phys. Rev. B* **5**, 2897–2924 (1972).
84. Yuan, Z. *Electrical Conductivity from First Principles*. Thesis, Humboldt-Universität zu (2022); https://hdl.handle.net/21.11116/0000-000A-FA8B-0.
85. Kietzmann, A., Holst, B., Redmer, R., Desjarlais, M. P. & Mattsson, T. R. Quantum molecular dynamics simulations for the nonmetal-to-metal transition in fluid helium. *Phys. Rev. Lett.* **98**, 190602 (2007).
86. Alfè, D., Pozzo, M. & Desjarlais, M. P. Lattice electrical resistivity of magnetic bcc iron from first-principles calculations. *Phys. Rev. B* **85**, 024102 (2012).
87. Gonze, X. et al. ABINIT: first-principles approach to material and nanosystem properties. *Comput. Phys. Commun.* **180**, 2582–2615 (2009).
88. Calderin, L., Karasiev, V. V. & Trickey, S. B. Kubo–Greenwood electrical conductivity formulation and implementation for projector augmented wave datasets. *Comput. Phys. Commun.* **221**, 118–142 (2017).
89. Di Paola, C., Macheda, F., Laricchia, S., Weber, C. & Bonini, N. First-principles study of electronic transport and structural properties of $Cu_{12}Sb_4S_{13}$ in its high-temperature phase. *Phys. Rev. Res.* **2**, 033055 (2020).
90. Knoop, F., Purcell, T., Scheffler, M. & Carbogno, C. FHI-vibes: ab initio vibrational simulations. *J. Open Source Softw.* **5**, 2671 (2020).
91. Pickem, M., Maggio, E. & Tomczak, J. M. Prototypical many-body signatures in transport properties of semiconductors. *Phys. Rev. B* **105**, 085139 (2022).
92. Landauer, R. Spatial variation of currents and fields due to localized scatterers in metallic conduction. *IBM J. Res. Dev.* **1**, 223–231 (1957).
First description of the general Landauer theory use for transport calculation.
93. Büttiker, M. Four-terminal phase-coherent conductance. *Phys. Rev. Lett.* **57**, 1761–1764 (1986).
Extension of the Landauer theory to multi-terminal by Büttiker.
94. Buttiker, M. Symmetry of electrical conduction. *IBM J. Res. Dev.* **32**, 317–334 (1988).
95. Sivan, U. & Imry, Y. Multichannel Landauer formula for thermoelectric transport with application to thermopower near the mobility edge. *Phys. Rev. B* **33**, 551–558 (1986).
96. Butcher, P. N. Thermal and electrical transport formalism for electronic microstructures with many terminals. *J. Phys. Condens. Matter.* **2**, 4869–4878 (1990).
97. Rudderham, C. & Maassen, J. Analysis of simple scattering models on the thermoelectric performance of analytical electron dispersions. *J. Appl. Phys.* **127**, 065105 (2020).
98. Rudderham, C. & Maassen, J. Ab initio thermoelectric calculations of ring-shaped bands in two-dimensional Bi_2Te_3, Bi_2Se_3, and Sb_2Te_3: comparison of scattering approximations. *Phys. Rev. B* **103**, 165406 (2021).
99. Wickramaratne, D., Zahid, F. & Lake, R. K. Electronic and thermoelectric properties of van der Waals materials with ring-shaped valence bands. *J. Appl. Phys.* **118**, 075101 (2015).
100. Diznab, M. R., Johnson, E. R. & Maassen, J. Periodic trends in the structural, electronic, and transport properties of electrenes. *Nanoscale* **15**, 12038–12047 (2023).
101. Kim, R., Datta, S. & Lundstrom, M. S. Influence of dimensionality on thermoelectric device performance. *J. Appl. Phys.* **105**, 034506 (2009).
102. Jeong, C., Kim, R., Luisier, M., Datta, S. & Lundstrom, M. On Landauer versus Boltzmann and full band versus effective mass evaluation of thermoelectric transport coefficients. *J. Appl. Phys.* **107**, 023707 (2010).
Comparison of Landauer–Boltzmann transport equation in the diffusive regime and the different expressions for the computation of thermoelectric properties.
103. Musland, L. & Flage-Larsen, E. Thermoelectric transport calculations using the Landauer approach, ballistic quantum transport simulations, and the Buttiker approximation. *Comput. Mater. Sci.* **132**, 146–157 (2017).
104. Smogunov, A., Corso, A. D. & Tosatti, E. Ballistic conductance of magnetic Co and Ni nanowires with ultrasoft pseudopotentials. *Phys. Rev. B* **70**, 045417 (2004).
105. Choi, H. J. & Ihm, J. Ab initio pseudopotential method for the calculation of conductance in quantum wires. *Phys. Rev. B* **59**, 2267–2275 (1999).
106. Stefanucci, G., van Leeuwen, R. & Perfetto, E. In and out-of-equilibrium ab initio theory of electrons and phonons. *Phys. Rev. X* **13**, 031026 (2023).
107. Kadanoff, L. & Baym, G. *Quantum Statistical Mechanics* (W.A. Benjamin Inc., 1962).
108. Papior, N., Lorente, N., Frederiksen, T., García, A. & Brandbyge, M. Improvements on non-equilibrium and transport Green function techniques: the next-generation TRANSIESTA. *Comput. Phys. Commun.* **212**, 8–24 (2017).
109. Frederiksen, T., Paulsson, M., Brandbyge, M. & Jauho, A.-P. Inelastic transport theory from first principles: methodology and application to nanoscale devices. *Phys. Rev. B* **75**, 205413 (2007).
110. Paulsson, M. & Brandbyge, M. Transmission eigenchannels from nonequilibrium Green's functions. *Phys. Rev. B* **76**, 115117 (2007).
111. Gustafsson, A. & Paulsson, M. Scanning tunneling microscopy current from localized basis orbital density functional theory. *Phys. Rev. B* **93**, 115434 (2016).
112. Avriller, R. & Frederiksen, T. Inelastic shot noise characteristics of nanoscale junctions from first principles. *Phys. Rev. B* **86**, 155411 (2012).
113. Gunst, T., Markussen, T., Palsgaard, M. L. N., Stokbro, K. & Brandbyge, M. First-principles electron transport with phonon coupling: large scale at low cost. *Phys. Rev. B* **96**, 161404 (2017).
114. Taylor, J., Guo, H. & Wang, J. Ab initio modeling of quantum transport properties of molecular electronic devices. *Phys. Rev. B* **63**, 245407 (2001).
115. *NanoDCAL Package* (Nanoacademic Technologies, 2024); https://nanoacademic.com/solutions/nanodcal/.
116. Pashov, D. et al. Questaal: a package of electronic structure methods based on the linear muffin-tin orbital technique. *Comput. Phys. Commun.* **249**, 107065 (2020).
117. Grange, T. Electron transport in quantum wire superlattices. *Phys. Rev. B* **89**, 165310 (2014).
118. Skylaris, C.-K., Haynes, P. D., Mostofi, A. A. & Payne, M. C. Introducing ONETEP: linear-scaling density functional simulations on parallel computers. *J. Chem. Phys.* **122**, 084119 (2005).
119. Bell, R. A., Dubois, S. M.-M., Payne, M. C. & Mostofi, A. A. Electronic transport calculations in the ONETEP code: implementation and applications. *Comput. Phys. Commun.* **193**, 78–88 (2015).

120. Rim, K., Narasimha, S., Longstreet, M., Mocuta, A. & Cai, J. Low field mobility characteristics of sub-100 nm unstrained and strained Si MOSFETs. In *International Electron Devices Meeting* IEDM-02 (IEEE, 2002); https://doi.org/10.1109/IEDM.2002.1175775.
121. Luisier, M. & Klimeck, G. Atomistic full-band simulations of silicon nanowire transistors: effects of electron–phonon scattering. *Phys. Rev. B* **80**, 155430 (2009).
122. Szabó, A., Rhyner, R. & Luisier, M. Ab initio simulation of single- and few-layer MoS_2 transistors: effect of electron–phonon scattering. *Phys. Rev. B* **92**, 035435 (2015).
123. Backman, J., Lee, Y. & Luisier, M. Phonon-limited transport in two-dimensional materials: a unified approach for ab initio mobility and current calculations. *Phys. Rev. Appl.* **21**, 054017 (2024).
124. Ye, M., Jiang, X., Li, S.-S. & Wang, L.-W. Large-scale first-principles quantum transport simulations using plane wave basis set on high performance computing platforms. *Comput. Phys. Commun.* **260**, 107737 (2021).
125. Ferretti, A., Bonferroni, B., Calzolari, A. & Nardelli, M. B. *WanT Package* (GitHub, 2023); https://github.com/QEF/want.
126. Ma, J., Nissimagoudar, A. S. & Li, W. First-principles study of electron and hole mobilities of Si and GaAs. *Phys. Rev. B* **97**, 045201 (2018).
127. Gao, S., Zhou, J.-J., Luo, Y. & Bernardi, M. First-principles electron–phonon interactions and electronic transport in large-angle twisted bilayer graphene. *Phys. Rev. Mater.* **8**, L051001 (2024).
128. Heyd, J., Scuseria, G. E. & Ernzerhof, M. Hybrid functionals based on a screened coulomb potential. *J. Chem. Phys.* **118**, 8207–8215 (2003).
129. Furness, J. W., Kaplan, A. D., Ning, J., Perdew, J. P. & Sun, J. Accurate and numerically efficient r2scan meta-generalized gradient approximation. *J. Phys. Chem. Lett.* **11**, 8208–8215 (2020).
130. Neophytou, N. *Theory and Simulation Methods for Electronic and Phononic Transport in Thermoelectric Materials* (Springer, 2020); https://doi.org/10.1007/978-3-030-38681-8.
131. Bloch, F. Zum elektrischen widerstandsgesetz bei tiefen temperaturen. *Zeitschrift für Physik* **59**, 208–214 (1930).
132. Peierls, R. Zur theorie der elektrischen und thermischen leitfähigkeit von metallen. *Ann. Phys.* **396**, 121–148 (1930).
133. Protik, N. H. & Broido, D. A. Coupled transport of phonons and carriers in semiconductors: a case study of n-doped GaAs. *Phys. Rev. B* **101**, 075202 (2020).
General coupled electron–phonon Boltzmann transport equation designed to capture the electron-drag and phonon-drag effects.
134. Protik, N. H., Li, C., Pruneda, M., Broido, D. & Ordejón, P. The elphbolt ab initio solver for the coupled electron–phonon Boltzmann transport equations. *npj Comput. Mater.* **8**, 28 (2022).
135. Protik, N. H. & Kozinsky, B. Electron–phonon drag enhancement of transport properties from a fully coupled ab initio Boltzmann formalism. *Phys. Rev. B* **102**, 245202 (2020).
136. Stefanucci, G. & Perfetto, E. Semiconductor electron–phonon equations: a rung above Boltzmann in the many-body ladder. *SciPost Phys.* **16**, 073 (2024).
137. Zhou, J. et al. Ab initio optimization of phonon drag effect for lower-temperature thermoelectric energy conversion. *Proc. Natl Acad. Sci. USA* **112**, 14777–14782 (2015).
138. Herring, C. Theory of the thermoelectric power of semiconductors. *Phys. Rev.* **96**, 1163–1187 (1954).
139. Pokharel, M. et al. Phonon drag effect in nanocomposite $FeSb_2$. *MRS Commun.* **3**, 31–36 (2013).
140. Weber, L. & Gmelin, E. Transport properties of silicon. *Appl. Phys. A* **53**, 136–140 (1991).
141. Frederikse, H. P. R. & Mielczarek, E. V. Thermoelectric power of indium antimonide. *Phys. Rev.* **99**, 1889–1890 (1955).
142. Yalamarthy, A. S. et al. Significant phonon drag enables high power factor in the AlGaN/GaN two-dimensional electron gas. *Nano Lett.* **19**, 3770–3776 (2019).
143. Zhou, J. et al. First-principles simulation of electron transport and thermoelectric property of materials, including electron–phonon scattering, defect scattering, and phonon drag https://archive.materialscloud.org/record/2020.106 (2020).
144. Novoselov, K. S. et al. Electric field effect in atomically thin carbon films. *Science* **306**, 666–669 (2004).
145. Butler, S. Z. et al. Progress, challenges, and opportunities in two-dimensional materials beyond graphene. *ACS Nano* **7**, 2898–2926 (2013).
146. Poncé, S., Schlipf, M. & Giustino, F. Origin of low carrier mobilities in halide perovskites. *ACS Energy Lett.* **4**, 456–463 (2019).
147. Rivano, N. *Phonons, Electron–Phonon Coupling and Charge Transport in Low-dimensional Materials*. PhD thesis, EPFL (2023). http://infoscience.epfl.ch/record/302181.
148. Böer, K. W. & Pohl, U. W. in *Semiconductor Physics* 1017–1051 (Springer, 2018); https://doi.org/10.1007/978-3-319-69150-3_27.
149. Sohier, T., Campi, D., Marzari, N. & Gibertini, M. Mobility of two-dimensional materials from first principles in an accurate and automated framework. *Phys. Rev. Mater.* **2**, 114010 (2018).
150. Troeye, B. V., Sankaran, K., Tokei, Z., Adelmann, C. & Pourtois, G. First-principles investigation of thickness-dependent electrical resistivity for low-dimensional interconnects. *Phys. Rev. B* **108**, 125117 (2023).
151. Zhou, M., Chen, X., Li, M. & Du, A. Widely tunable and anisotropic charge carrier mobility in monolayer tin(ii) selenide using biaxial strain: a first-principles study. *J. Mater. Chem. C* **5**, 1247–1254 (2017).
152. Lang, H., Zhang, S. & Liu, Z. Mobility anisotropy of two-dimensional semiconductors. *Phys. Rev. B* **94**, 235306 (2016).
153. Qiao, J., Kong, X., Hu, Z.-X., Yang, F. & Ji, W. High-mobility transport anisotropy and linear dichroism in few-layer black phosphorus. *Nat. Commun.* **5**, 4475 (2014).
154. Rivano, N., Marzari, N. & Sohier, T. Infrared-active phonons in one-dimensional materials and their spectroscopic signatures. *npj Comput. Mater.* **9**, 194 (2023).
155. Choi, A. Y., Cheng, P. S., Hatanpää, B. & Minnich, A. J. Electronic noise of warm electrons in semiconductors from first principles. *Phys. Rev. Mater.* **5**, 044603 (2021).
156. Wang, S. et al. Comparison the electron momentum and energy relaxation process in wurtzite GaN, InN and AlN by Monte Carlo method. *Solid State Commun.* **288**, 68–73 (2019).
157. Lee, N.-E., Zhou, J.-J., Chen, H.-Y. & Bernardi, M. Ab initio electron-two-phonon scattering in GaAs from next-to-leading order perturbation theory. *Nat. Commun.* **11**, 1607 (2020).
158. Hatanpää, B., Choi, A. Y., Cheng, P. S. & Minnich, A. J. Two-phonon scattering in nonpolar semiconductors: a first-principles study of warm electron transport in Si. *Phys. Rev. B* **107**, L041110 (2023).
159. Cheng, P. S., Sun, J., Sun, S.-N., Choi, A. Y. & Minnich, A. J. High-field transport and hot-electron noise in GaAs from first-principles calculations: role of two-phonon scattering. *Phys. Rev. B* **106**, 245201 (2022).
160. Aninkevicius, V. et al. Hot-electron noise and diffusion in AlGaAs/GaAs. *Semicond. Sci. Technol.* **9**, 576–579 (1994).
161. Hartnagel, H., Katilius, R. & Matulionis, A. *Microwave Noise in Semiconductor Devices* (John Wiley & Sons, 2001); https://api.semanticscholar.org/CorpusID:118611130.
162. Fischetti, M. V., DiMaria, D. J., Brorson, S. D., Theis, T. N. & Kirtley, J. R. Theory of high-field electron transport in silicon dioxide. *Phys. Rev. B* **31**, 8124–8142 (1985).
163. Fawcett, W., Boardman, A. & Swain, S. Monte Carlo determination of electron transport properties in gallium arsenide. *J. Phys. Chem. Solids* **31**, 1963–1990 (1970).
164. la Torre, I. I., Mateos, J., Pardo, D. & González, T. Monte Carlo analysis of noise spectra in self-switching nanodiodes. *J. Appl. Phys.* **103**, 024502 (2008).
165. Rodilla, H. et al. Cryogenic performance of low-noise InP HEMTs: a Monte Carlo study. *IEEE Trans. Electron Devices* **60**, 1625–1631 (2013).
166. Mateos, J., Rodilla, H., Vasallo, B. G. & González, T. Monte Carlo modelling of noise in advanced III–V HEMTs. *J. Comput. Electron.* **14**, 72–86 (2014).
167. Ghosh, K. & Singisetti, U. Ab initio velocity-field curves in monoclinic β-Ga_2O_3. *J. Appl. Phys.* **122**, 035702 (2017).
168. Maliyov, I., Park, J. & Bernardi, M. Ab initio electron dynamics in high electric fields: accurate prediction of velocity-field curves. *Phys. Rev. B* **104**, L100303 (2021).
169. Catherall, D. S. & Minnich, A. J. High-field charge transport and noise in *p*-Si from first principles. *Phys. Rev. B* **107**, 035201 (2023).
170. Kingon, A. I., Maria, J.-P. & Streiffer, S. K. Alternative dielectrics to silicon dioxide for memory and logic devices. *Nature* **406**, 1032–1038 (2000).
171. Li, T., Wan, B., Du, G., Zhang, B. & Zeng, Z. Electrical performance of multilayer MoS_2 transistors on high-κ Al_2O_3 coated si substrates. *AIP Adv.* **5**, 057102 (2015).
172. Jena, D. & Konar, A. Enhancement of carrier mobility in semiconductor nanostructures by dielectric engineering. *Phys. Rev. Lett.* **98**, 136805 (2007).
173. Radisavljevic, B., Radenovic, A., Brivio, J., Giacometti, V. & Kis, A. Single-layer MoS_2 transistors. *Nat. Nanotechnol.* **6**, 147–150 (2011).
174. Kaasbjerg, K., Thygesen, K. S. & Jacobsen, K. W. Phonon-limited mobility in *n*-type single-layer MoS_2 from first principles. *Phys. Rev. B* **85**, 115317 (2012).
175. Fischetti, M. V., Neumayer, D. A. & Cartier, E. A. Effective electron mobility in Si inversion layers in metal–oxide–semiconductor systems with a high-κ insulator: the role of remote phonon scattering. *J. Appl. Phys.* **90**, 4587–4608 (2001).
Effect of remote phonon scattering on the mobility of Si with high dielectrics.
176. Gopalan, S., Van de Put, M. L., Gaddemane, G. & Fischetti, M. V. Theoretical study of electronic transport in two-dimensional transition metal dichalcogenides: effects of the dielectric environment. *Phys. Rev. Appl.* **18**, 054062 (2022).
177. Ma, Y. X., Su, H., Tang, W. M. & Lai, P. T. Review on remote phonon scattering in transistors with metal-oxide-semiconductor structures adopting high-κ gate dielectrics. *J. Vac. Sci. Technol. B* **41**, 060804 (2023).
178. Hess, K. & Vogl, P. Remote polar phonon scattering in silicon inversion layers. *Solid State Commun.* **30**, 797–799 (1979).
179. Fischetti, M. V. & Laux, S. E. Monte carlo study of electron transport in silicon inversion layers. *Phys. Rev. B* **48**, 2244–2274 (1993).
180. O'Regan, T. & Fischetti, M. Electron mobility in silicon and germanium inversion layers: the role of remote phonon scattering. *J. Comput. Electron.* **6**, 81–84 (2007).
181. Zhang, Y., Fischetti, M. V., Sorée, B. & O'Regan, T. Theory of hole mobility in strained Ge and III–V p-channel inversion layers with high-κ insulators. *J. Appl. Phys.* **108**, 123713 (2010).
182. Radisavljevic, B. & Kis, A. Mobility engineering and a metal–insulator transition in monolayer MoS_2. *Nat. Mater.* **12**, 815–820 (2013).
183. Groves, S. H., Pidgeon, C. R. & Feinleib, J. Infrared magnetoelectroreflectance in Ge, GaSb, and InSb. *Phys. Rev. Lett.* **17**, 643–646 (1966).
184. Zwerdling, S., Button, K. J., Lax, B. & Roth, L. M. Internal impurity levels in semiconductors: experiments in p-type silicon. *Phys. Rev. Lett.* **4**, 173–176 (1960).
185. Williams, E. W. & Rehn, V. Electroreflectance studies of InAs, GaAs, and (Ga,In) As alloys. *Phys. Rev.* **172**, 798–810 (1968).
186. Blacha, A., Cardona, M., Christensen, N., Ves, S. & Overhof, H. Volume dependence of the spin–orbit splitting in the copper halides. *Physica B+C* **117–118**, 63–65 (1983).

187. Hirohata, A. et al. Review on spintronics: principles and device applications. *J. Magnet. Magn. Mater.* **509**, 166711 (2020).
188. Stern, N. P., Berezovsky, J., Ghosh, S. & Awschalom, D. D. *Manipulation of Spins and Coherence in Semiconductors* (Wiley, 2007); https://doi.org/10.1002/9780470022184.hmm530.
189. Ahn, E. C. 2d materials for spintronic devices. *npj 2D Mater. Appl.* **4**, 17 (2020).
190. Xu, J. & Ping, Y. Ab initio predictions of spin relaxation, dephasing, and diffusion in solids. *J. Chem. Theory Comput.* **20**, 492–512 (2023).
191. Reticcioli, M., Diebold, U., Kresse, G. & Franchini, C. *Small Polarons in Transition Metal Oxides* (Springer, 2018); https://doi.org/10.1007/978-3-319-50257-1_52-1.
192. Devreese, J. T. Fröhlich Polarons. Lecture course including detailed theoretical derivations -- 10th edition. Preprint at https://arxiv.org/abs/1611.06122 (2016).
193. Miyata, K., Atallah, T. L. & Zhu, X.-Y. Lead halide perovskites: crystal-liquid duality, phonon glass electron crystals, and large polaron formation. *Sci. Adv.* **3**, e1701469 (2017).
194. Bosman, A. & van Daal, H. Small-polaron versus band conduction in some transition-metal oxides. *Adv. Phys.* **19**, 1–117 (1970).
Analysis of the transport behaviour of several transition-metal oxides showing that small polarons transport is linked with low mobility.
195. Marcus, R. A. On the theory of oxidation–reduction reactions involving electron transfer. I. *J. Chem. Phys.* **24**, 966–978 (1956).
196. Emin, D. & Holstein, T. Studies of small-polaron motion IV. Adiabatic theory of the Hall effect. *Ann. Phys.* **53**, 439–520 (1969).
197. Holstein, T. Studies of polaron motion. *Ann. Phys.* **281**, 725–773 (2000).
198. Austin, I. G. & Mott, N. F. Polarons in crystalline and non-crystalline materials. *Adv. Phys.* **50**, 757–812 (2001).
199. Jónsson, H., Mills, G. & Jacobsen, K. W. Nudged elastic band method for finding minimum energy paths of transitions. In *Classical and Quantum Dynamics in Condensed Phase Simulations* 385–404 (World Scientific, 1998).
200. Henkelman, G. & Jónsson, H. Improved tangent estimate in the nudged elastic band method for finding minimum energy paths and saddle points. *J. Chem. Phys.* **113**, 9978–9985 (2000).
201. Sheppard, D., Terrell, R. & Henkelman, G. Optimization methods for finding minimum energy paths. *J. Chem. Phys.* **128**, 134106 (2008).
202. Watthaisong, P., Jungthawan, S., Hirunsit, P. & Suthirakun, S. Transport properties of electron small polarons in a V_2O_5 cathode of Li-ion batteries: a computational study. *RSC Adv.* **9**, 19483–19494 (2019).
203. Adelstein, N., Neaton, J. B., Asta, M. & De Jonghe, L. C. Density functional theory based calculation of small-polaron mobility in hematite. *Phys. Rev. B* **89**, 245115 (2014).
204. Luong, H. D., Tran, T. L., Phung, V. B. T. & Dinh, V. A. Small polaron transport in cathode materials of rechargeable ion batteries. *J. Sci. Adv. Mater. Dev.* **7**, 100410 (2022).
205. Morita, K., Golomb, M. J., Rivera, M. & Walsh, A. Models of polaron transport in inorganic and hybrid organic–inorganic titanium oxides. *Chem. Mater.* **35**, 3652–3659 (2023).
206. Reticcioli, M., Setvin, M., Schmid, M., Diebold, U. & Franchini, C. Formation and dynamics of small polarons on the rutile TiO_2 (110) surface. *Phys. Rev. B* **98**, 045306 (2018).
207. Setvin, M. et al. Direct view at excess electrons in TiO_2 rutile and anatase. *Phys. Rev. Lett.* **113**, 086402 (2014).
208. Fratini, S. & Ciuchi, S. Dynamical mean-field theory of transport of small polarons. *Phys. Rev. Lett.* **91**, 256403 (2003).
209. Emin, D. Polarons in condensed matter. Preprint at https://arxiv.org/abs/2205.02878 (2022).
210. Grundmann, M. *The Physics of Semiconductors* (Springer, 2016); https://doi.org/10.1007/978-3-319-23880-7.
211. Franchini, C., Reticcioli, M., Setvin, M. & Diebold, U. Polarons in materials. *Nat. Rev. Mater.* **6**, 560–586 (2021).
Review on polarons, their effects in materials and the range of experimental and computational approaches to describe them.
212. Kadanoff, L. P. Boltzmann equation for polarons. *Phys. Rev.* **130**, 1364–1369 (1963).
213. Feynman, R. P., Hellwarth, R. W., Iddings, C. K. & Platzman, P. M. Mobility of slow electrons in a polar crystal. *Phys. Rev.* **127**, 1004–1017 (1962).
214. Hellwarth, R. W. & Biaggio, I. Mobility of an electron in a multimode polar lattice. *Phys. Rev. B* **60**, 299–307 (1999).
215. Frost, J. M. Calculating polaron mobility in halide perovskites. *Phys. Rev. B* **96**, 195202 (2017).
216. Chang, B. K., Zhou, J.-J., Lee, N.-E. & Bernardi, M. Intermediate polaronic charge transport in organic crystals from a many-body first-principles approach. *npj Comput. Mater.* **8**, 63 (2022).
217. Sio, W. H., Verdi, C., Poncé, S. & Giustino, F. Polarons from first principles, without supercells. *Phys. Rev. Lett.* **122**, 246403 (2019).
218. Sio, W. H., Verdi, C., Poncé, S. & Giustino, F. Ab initio theory of polarons: formalism and applications. *Phys. Rev. B* **99**, 235139 (2019).
219. Giustino, F., Louie, S. G. & Cohen, M. L. Electron–phonon renormalization of the direct band gap of diamond. *Phys. Rev. Lett.* **105**, 265501 (2010).
220. Zhang, Y., Wang, Z., Xi, J. & Yang, J. Temperature-dependent band gaps in several semiconductors: from the role of electron–phonon renormalization. *J. Phys. Condens. Matter.* **32**, 475503 (2020).
221. Poncé, S. et al. Temperature dependence of the electronic structure of semiconductors and insulators. *J. Chem. Phys.* **143**, 102813 (2015).
222. Floris, A., de Gironcoli, S., Gross, E. K. U. & Cococcioni, M. Vibrational properties of MnO and NiO from DFT+U-based density functional perturbation theory. *Phys. Rev. B* **84**, 161102 (2011).
223. Floris, A. et al. Hubbard-corrected density functional perturbation theory with ultrasoft pseudopotentials. *Phys. Rev. B* **101**, 064305 (2020).
224. Zhou, J.-J. et al. Ab initio electron–phonon interactions in correlated electron systems. *Phys. Rev. Lett.* **127**, 126404 (2021).
225. Abramovitch, D. J., Mravlje, J., Zhou, J.-J., Georges, A. & Bernardi, M. Respective roles of electron–phonon and electron–electron interactions in the transport and quasiparticle properties of $SrVO_3$. *Phys. Rev. Lett.* **133**, 186501 (2024).
226. Chang, B. K. et al. First-principles electron–phonon interactions and polarons in the parent cuprate La_2CuO_4. Preprint at https://arxiv.org/abs/2401.11322 (2024).
227. Li, Z., Antonius, G., Wu, M., da Jornada, F. H. & Louie, S. G. Electron–phonon coupling from ab initio linear-response theory within the GW method: correlation-enhanced interactions and superconductivity in $Ba_{1-x}K_xBiO_3$. *Phys. Rev. Lett.* **122**, 186402 (2019).
228. Li, Z., Antonius, G., Chan, Y.-H. & Louie, S. G. Electron–phonon coupling from GW perturbation theory: practical workflow combining BerkeleyGW, ABINIT, and EPW. *Comput. Phys. Commun.* **295**, 109003 (2024).
229. Monserrat, B. Electron–phonon coupling from finite differences. *J. Phys. Condens. Matter.* **30**, 083001 (2018).
230. Müller, M. C. T. D., Blügel, S. & Friedrich, C. Electron–magnon scattering in elementary ferromagnets from first principles: lifetime broadening and band anomalies. *Phys. Rev. B* **100**, 045130 (2019).
231. Nabok, D., Blügel, S. & Friedrich, C. Electron–plasmon and electron–magnon scattering in ferromagnets from first principles by combining GW and GT self-energies. *npj Comput. Mater.* **7**, 178 (2021).
232. Katsnelson, M. I., Irkhin, V. Y., Chioncel, L., Lichtenstein, A. I. & de Groot, R. A. Half-metallic ferromagnets: from band structure to many-body effects. *Rev. Mod. Phys.* **80**, 315–378 (2008).
233. Irkhin, V. Y. & Irkhin, Y. P. *Electronic Structure, Correlation Effects and Physical Properties of d- and f-Metals and Their Compounds* (Cambridge International Science Publishing, 2007).
234. Badrtdinov, D. I., Pushkarev, G. V., Katsnelson, M. I. & Rudenko, A. N. Electron transport and scattering mechanisms in ferromagnetic monolayer Fe_3GeTe_2. *npj 2D Mater. Appl.* **7**, 52 (2023).
235. Haldar, A., Clark, Q., Zacharias, M., Giustino, F. & Sharifzadeh, S. Machine learning electron–phonon interactions in 2D materials. Preprint at https://doi.org/10.21203/rs.3.rs-3253133/v1 (2023).
236. Li, H. et al. Deep-learning density functional perturbation theory. *Phys. Rev. Lett.* **132**, 096401 (2024).
237. Graziosi, P., Li, Z. & Neophytou, N. Electra code: full-band electronic transport properties of materials. *Comput. Phys. Commun.* **287**, 108670 (2023).
238. Rhyner, R. & Luisier, M. Phonon-limited low-field mobility in silicon: quantum transport vs. linearized Boltzmann transport equation. *J. Appl. Phys.* **114**, 223708 (2013).
239. Restrepo, O. D., Varga, K. & Pantelides, S. T. First-principles calculations of electron mobilities in silicon: phonon and coulomb scattering. *Appl. Phys. Lett.* **94**, 212103 (2009).
240. Canali, C., Jacoboni, C., Nava, F., Ottaviani, G. & Alberigi-Quaranta, A. Electron drift velocity in silicon. *Phys. Rev. B* **12**, 2265–2284 (1975).
241. Markussen, T. et al. Electron–phonon scattering from Green's function transport combined with molecular dynamics: applications to mobility predictions. *Phys. Rev. B* **95**, 245210 (2017).
242. Jacoboni, C., Canali, C., Ottaviani, G. & Alberigi Quaranta, A. A review of some charge transport properties of silicon. *Solid-State Electron.* **20**, 77–89 (1977).
243. Madelung, O. et al. *Group IV Elements, IV–IV and III–V Compounds. Part b — Electronic, Transport, Optical and Other Properties* (Springer-Verlag, 2002); https://doi.org/10.1007/b80447.
244. Sze, S. M. *Semiconductor Devices: Physics and Technology* (John Wiley & Sons, 2008).
245. Szmulowicz, F. Calculation of optical- and acoustic-phonon-limited conductivity and Hall mobilities for *p*-type silicon and germanium. *Phys. Rev. B* **28**, 5943–5963 (1983).
246. Gaddemane, G., Gopalan, S., Van de Put, M. L. & Fischetti, M. V. Limitations of ab initio methods to predict the electronic-transport properties of two-dimensional semiconductors: the computational example of 2H-phase transition metal dichalcogenides. *J. Comput. Electron.* **20**, 49–59 (2020).
247. Deng, T. et al. Ab initio dipolar electron–phonon interactions in two-dimensional materials. *Phys. Rev. B* **103**, 075410 (2021).
248. Zhao, Y. et al. Intrinsic electronic transport and thermoelectric power factor in n-type doped monolayer MoS_2. *N. J. Phys.* **20**, 043009 (2018).
249. Restrepo, O. D., Krymowski, K. E., Goldberger, J. & Windl, W. A first principles method to simulate electron mobilities in 2D materials. *N. J. Phys.* **16**, 105009 (2014).
250. Chaudhuri, S., Bhattacharya, A., Das, A., Das, G. & Dev, B. Strain driven anomalous anisotropic enhancement in the thermoelectric performance of monolayer MoS_2. *Appl. Surf. Sci.* **626**, 157139 (2023).
251. Li, X. et al. Intrinsic electrical transport properties of monolayer silicene and MoS_2 from first principles. *Phys. Rev. B* **87**, 115418 (2013).
252. Yoon, Y., Ganapathi, K. & Salahuddin, S. How good can monolayer MoS_2 transistors be? *Nano Lett.* **11**, 3768–3773 (2011).

253. Yu, Z. et al. Towards intrinsic charge transport in monolayer molybdenum disulfide by defect and interface engineering. *Nat. Commun.* **5**, 5290 (2014).
254. Liu, Y. et al. Toward barrier free contact to molybdenum disulfide using graphene electrodes. *Nano Lett.* **15**, 3030–3034 (2015).
255. Yu, Z. et al. Realization of room-temperature phonon-limited carrier transport in monolayer MoS_2 by dielectric and carrier screening. *Adv. Mater.* **28**, 547–552 (2015).

Acknowledgements
The authors thank M. Giantomassi for the fruitful discussions and for his help throughout the writing of this Review. R.C. acknowledges financial support from the Communauté Française de Belgique, grant ARC 18/23-093. G.-M.R. and S.P. acknowledge financial support from the Fonds de la Recherche Scientifique de Belgique (FRS-FNRS). Computational resources have been provided by the Consortium des Équipements de Calcul Intensif, funded by the FRS-FNRS under Grant No. 2.5020.11 and by the Walloon Region. The present research benefited from computational resources made available on the Tier-1 supercomputer of the Fédération Wallonie-Bruxelles, infrastructure funded by the Walloon Region under Grant No. 1117545. G.H. acknowledges funding by the US Department of Energy, Office of Science, Basic Energy Sciences under award number DE-SC0023509. The work has received partial support from the European Union's Horizon 2020 research and innovation programme, Grant No. 951786 through the Center of Excellence NOMAD.

Author contributions
All authors contributed equally to this work.

Competing interests
The authors declare no competing interests.

Additional information
Peer review information *Nature Reviews Physics* thanks Massimo Fischetti and the other, anonymous, reviewer(s) for their contribution to the peer review of this work.

Publisher's note Springer Nature remains neutral with regard to jurisdictional claims in published maps and institutional affiliations.